Published for SISSA by Springer

Received: *September 11, 2024*
Revised: *January 22, 2025*
Accepted: *February 24, 2025*
Published: *March 20, 2025*

Jet veto resummation for STXS H+1-jet bins at aNNLL′+NNLO

Pedro Cal,[a] **Matthew A. Lim**,[b] **Darren J. Scott**,[c] **Frank J. Tackmann**[a] **and Wouter J. Waalewijn**[d,e]

[a] *Deutsches Elektronen-Synchrotron DESY, Notkestr. 85, 22607 Hamburg, Germany*
[b] *Department of Physics and Astronomy, University of Sussex, Sussex House, Brighton, BN1 9RH, U.K.*
[c] *Max Planck Institute for Physics, Boltzmannstr. 8 D-85748 Garching, Germany*
[d] *Institute for Theoretical Physics Amsterdam and Delta Institute for Theoretical Physics, University of Amsterdam, Science Park 904, 1098 XH Amsterdam, The Netherlands*
[e] *Nikhef, Theory Group, Science Park 105, 1098 XG, Amsterdam, The Netherlands*
E-mail: pedro.cal@desy.de, m.a.lim@sussex.ac.uk, dscott@mpp.mpg.de, frank.tackmann@desy.de, w.j.waalewijn@uva.nl

Abstract: Measurements of Higgs boson processes by the ATLAS and CMS experiments at the LHC use Simplified Template Cross Sections (STXS) as a common framework for the combination of measurements in different decay channels and their further interpretation, e.g. to measure Higgs couplings. The different Higgs production processes are measured in predefined kinematic regions — the STXS bins — requiring precise theory predictions for each individual bin. In gluon-fusion Higgs production a main division is into 0-jet, 1-jet, and $\geq$ 2-jet bins, which are further subdivided in bins of the Higgs transverse momentum p_T^H. Requiring a fixed number of jets induces logarithms $\ln p_T^{\text{cut}}/Q$ in the cross section where p_T^{cut} is the jet-p_T threshold and $Q \sim p_T^H \sim m_H$ the hard-interaction scale. These jet-veto logarithms can be resummed to all orders in perturbation theory to achieve the highest possible perturbative precision. We provide state-of-the art predictions for the p_T^H spectrum in exclusive H+1-jet production and the corresponding H+1-jet STXS bins in the kinematic regime $p_T^{\text{cut}} \ll p_T^H \sim m_H$. We carry out the resummation at NNLL′ accuracy, using theory nuisance parameters to account for the few unknown ingredients at this order, and match to full NNLO. We revisit the jet-veto factorization for this process and find that it requires refactorizing the total soft function into a global and soft-collinear contribution in order to fully account for logarithms of the signal jet radius. The leading nonglobal logarithms are also included, though they are numerically small for the region of phenomenological interest.

Keywords: Factorization, Renormalization Group, Higgs Production, Jets and Jet Substructure, Resummation

ArXiv ePrint: 2408.13301

https://doi.org/10.1007/JHEP03(2025)155

Contents

1 Introduction

Since the discovery of the Higgs boson [1, 2], a major goal of the LHC physics programme has been to measure its properties by leveraging all available production and decay channels. For this purpose, the ATLAS and CMS experiments have adopted Simplified Template Cross Sections (STXS) [3–5] as a common framework. It is designed to maximize the experimental sensitivity by allowing the combination of measurements in different decay channels and experiments. At the same time it aims to minimize the theory or model dependence in the measurements by dividing the different Higgs production cross sections into predefined and mutually exclusive kinematic regions called the STXS bins. For the latest STXS measurements from Run 2 see e.g. refs. [6–8].

For the dominant Higgs production channel (via gluon fusion), the cross section is first divided into $p_T^H < 200\,\text{GeV}$ and $p_T^H > 200\,\text{GeV}$ bins, where p_T^H is the transverse momentum of the Higgs boson. The $p_T^H > 200\,\text{GeV}$ bin primarily targets boosted Higgs production which is sensitive to possible BSM effects. Most of the cross section lies in the $p_T^H < 200\,\text{GeV}$ bin, which is split into exclusive 0-jet, exclusive 1-jet, and inclusive $\geq$ 2-jets bins. The 0-jet and 1-jet bins are further split into p_T^H bins. To make maximal use of the STXS measurements, precise theory predictions for the cross section in each bin are required.

JHEP03(2025)155

Requiring a fixed number of jets, as is the case for the 0-jet and 1-jet bins, means that additional jets above some transverse momentum threshold p_T^{cut} are vetoed. For typical values of $p_T^{\text{cut}} \sim 25 - 30\,\text{GeV}$, the jet veto constrains the phase space for additional emissions quite strongly, which induces logarithms $\ln p_T^{\text{cut}}/Q$ in the cross section where $Q \sim p_T^H \sim m_H$ is a typical hard-interaction scale. The best possible perturbative precision is then achieved by resumming the jet-veto logarithms to all orders in perturbation theory.

The resummation for colour-singlet processes such as Drell-Yan or gluon-fusion Higgs production in the 0-jet limit was first derived in refs. [9–11] using the beam thrust event shape. The factorization and resummation for the leading-jet p_T was derived in refs. [12–15], and resummed results for the corresponding 0-jet cross section up to NNLL′ order matched to either fixed NNLO or N^{3}LO are available [16–18]. The 0-jet resummation has also been carried out for other colour-singlet processes [19–29], and also including an additional cut on the jet rapidity [30] or a smooth weighting with the jet rapidity [31, 32]. In ref. [33], the 0-jet resummation for the WW process was used to match NNLO predictions to a parton shower algorithm using the GENEVA framework [34, 35].

In this paper, we consider gluon-fusion Higgs production in association with one hard (signal) jet and a jet-p_T veto on additional jets, which we will refer to simply as H+1-jet production from here on. This is directly relevant for the gluon-fusion STXS 1-jet bins. In this case, the resummation is currently only available up to NLL′ [36–38].

We extend the resummation of jet-veto logarithms for H+1-jet to NNLL′ order matched to NNLO. A few of the required perturbative ingredients at NNLL′ are not yet available. They are parametrized in terms of theory nuisance parameters (TNPs) [39] and are treated as an additional source of uncertainty. Despite this, the resulting approximate resummation, denoted as aNNLL′, still allows us to reduce the perturbative uncertainty at aNNLL′+NNLO substantially compared to NLL′+NLO and to the pure NNLO. Here, aNNLL′ refers to the global jet veto logarithms — in the H+1-jet cross section there are additional nonglobal logarithms and clustering effects that will be discussed below. The uncertainties can be reduced further once the few remaining ingredients become known. Due to the lack of a public code for the NNLO calculation, we have obtained it indirectly from publicly available numerical results [40, 41]. In practice this is not a limitation, but a public code would of course facilitate the matching procedure.

Our resummation setup is valid in the kinematic regime where p_T^{cut} is considered parametrically small compared to any other scale $p_T^{\text{cut}} \ll p_T^J \sim p_T^H \sim m_H$, where p_T^J is the p_T of the leading jet. For $p_T^{\text{cut}} = 30\,\text{GeV}$, this allows us to obtain state-of-the-art resummed predictions for the p_T^H spectrum above $p_T^H \gtrsim 60\,\text{GeV}$ and the corresponding two STXS 1-jet bins with $p_T^H \in [60, 120]\,\text{GeV}$ and $p_T^H \in [120, 200]\,\text{GeV}$. On the other hand, for smaller p_T^H the more appropriate parametric hierarchy is $p_T^{\text{cut}} \sim p_T^H \sim p_T^J \ll m_H$. The resummation in this scenario requires a rather different setup, which we leave to future work.[1]

Compared to the 0-jet case, the presence of the additional signal jet in the final state substantially complicates the factorization structure. We therefore reconsider the derivation of the factorized cross section, focussing in particular on the all-order factorization of the measurement. Although the experimental analyses typically use the same jet radius for

[1] In principle, our results can be extended to smaller p_T^H at fixed order in a manner similar to ref. [38].

JHEP03(2025)155

both signal and vetoed jets, we find it important to distinguish between them, as it helps to clarify the structure of the logarithms and their factorization. We denote the jet radius of the signal jet by R_J and that of the vetoed jets by R_{cut}. The factorization is formally derived in the narrow-jet limit for both, i.e. $R_J^2, R_{\text{cut}}^2 \ll 1$. We also discuss how to include numerically important $\mathcal{O}(R_J^2)$ power corrections that are enhanced by jet-veto logarithms. Our resummation fully accounts for all logarithms of the jet radius R_J, which compared to refs. [36, 37] requires a further factorization of the total soft function into a global and soft-collinear contribution. The fact that emissions outside the signal jet are constrained whilst inside the jet they are unconstrained also leads to the appearance of nonglobal logarithms, that are not captured by the jet-veto factorization. Their numerical impact (at fixed order) was already observed to be minor in ref. [37]. Here, we also include a resummation of the leading nonglobal logarithms, finding that it has only a small numerical effect for the region of phenomenological interest.

Concerning the dependence on the jet-veto radius R_{cut}, the situation is analogous to the 0-jet case. The resummation of R_{cut} logarithms (so-called clustering logarithms) is a more delicate issue as explained in ref. [14]. Their leading resummation was achieved via numerical methods in refs. [18, 42], and it was shown to have a very small effect. For this reason, we do not attempt to include these effects here and only include the R_{cut} logarithms at fixed order. In principle, the results of ref. [18] could be included in our formalism via a suitable modification of the anomalous dimensions.

This work is organized as follows. In section 2, we discuss the factorization and resummation necessary to achieve NNLL′+NNLO accuracy for H+1-jet production. We begin by reviewing the Born kinematics in section 2.1, present the factorized cross section and corresponding building blocks in section 2.2 and discuss the factorization of the measurement in section 2.3. We give all required perturbative ingredients in section 3.1, and in section 3.2 we validate the singular structure of the factorized cross section, highlighting the importance of including power corrections in R_J^2 in the soft function. In sections 3.3 and 3.4, we discuss the details of the NNLL′ resummation and how we assess the perturbative uncertainties. We present our numerical results in section 4 and conclude in section 5.

2 Factorization

2.1 Kinematics

At Born level, the H+1-jet production process is a $2 \to 2$ scattering of the form

$$p_a + p_b \to p_J + p_H \,, \tag{2.1}$$

where p_a, p_b are the momenta of the incoming partons and p_J and p_H are the momenta of the signal jet and the Higgs boson. The Born kinematics are sufficient to describe the hard scattering processes, since the veto on additional jets prohibits additional *hard* real radiation. The kinematics are fully specified by the transverse momentum and rapidity of the signal jet, p_T^J and y_J, as well as the total rapidity of the system Y. The Mandelstam variables

JHEP03(2025)155

can be written in terms of these variables as

$$\begin{aligned} s_{ab} &\equiv (p_a + p_b)^2 = Q^2 \,, \\ s_{aJ} &\equiv (p_a - p_J)^2 = -p_T^J \, Q e^{Y - y_J} \,, \\ s_{bJ} &\equiv (p_b - p_J)^2 = -p_T^J \, Q e^{y_J - Y} \,, \end{aligned} \tag{2.2}$$

where we have used the partonic centre-of-mass energy Q, which is itself expressed in terms of p_T^J, Y, and y_J as

$$Q(p_T^J, Y, y_J) = p_T^J \cosh(y_J - Y) + \sqrt{(p_T^J)^2 \cosh^2(y_J - Y) + m_H^2} \,. \tag{2.3}$$

We will also make use of the initial-state parton momentum fractions x_a and x_b, and the large light-cone momenta associated with each of these, ω_a and ω_b. In terms of p_T^J, Y, and y_J (and equivalently Q) these are given by

$$x_a = \frac{\omega_a}{E_{\rm cm}} = \frac{Q}{E_{\rm cm}} \, e^{Y} \,, \qquad x_b = \frac{\omega_b}{E_{\rm cm}} = \frac{Q}{E_{\rm cm}} \, e^{-Y} \,. \tag{2.4}$$

The parametrization in terms of p_T^J, Y, and y_J is a natural one since the soft function depends on the rapidity of the jet (see section 3.1.4), which specifies the direction of its associated Wilson line. However, we are often interested in predictions for cross sections defined in terms of kinematic variables of the Higgs boson, rather than the jet. The change of variables from jet transverse momentum and rapidity to those of the Higgs, $(p_T^J, y_J) \to (p_T^H, y_H)$, can be performed in a straightforward manner. Due to the veto on additional jets, the transverse momentum of the Higgs boson is necessarily identical to that of the jet it recoils against (up to power corrections):

$$p_T^H = p_T^J \,. \tag{2.5}$$

The relation between y_H and (p_T^J, Y, y_J) is given by

$$y_H = y_J + \ln\left(\frac{Q e^{Y - y_J} - p_T^J}{E_T^H}\right), \tag{2.6}$$

where $E_T^H = \sqrt{(p_T^H)^2 + m_H^2}$ denotes the transverse energy of the Higgs boson.

For a given p_T^J, the kinematically allowed range for Y is

$$|Y| \leq \ln\left(\frac{E_{\rm cm}}{p_T^J + \sqrt{(p_T^J)^2 + m_H^2}}\right), \tag{2.7}$$

where the bound is saturated when $y_J = Y$. Similarly, for a given p_T^J and Y,

$$|y_J - Y| \leq \operatorname{arccosh}\left(\frac{e^{-|Y|}(E_{\rm cm}^2 - e^{2|Y|} m_H^2)}{2 E_{\rm cm} \, p_T^J}\right). \tag{2.8}$$

The limit on Y in eq. (2.7) ensures that the argument of the hyperbolic cosine in eq. (2.8) is always greater than or equal to one, such that $|y_J - Y|$ is always bounded by a positive real number. Likewise, when using Higgs kinematics, a similar set of constraints holds:

$$|Y| \leq \ln\left(\frac{E_{\rm cm}}{p_T^H + E_T^H}\right),$$

JHEP03(2025)155

Mode (n)	$p^\mu \sim (+,-,\perp)$	p^2
Beam (n_a, n_b)	$Q(\lambda^2, 1, \lambda)$	$Q^2\lambda^2$
Jet (n_J)	$Q(R_J^2, 1, R_J)$	$Q^2 R_J^2$
Soft	$Q\lambda(1,1,1)$	$Q^2\lambda^2$
Soft-collinear (n_J)	$Q\lambda(R_J^2, 1, R_J)$	$Q^2\lambda^2 R_J^2$

Table 1. Power counting of the modes present in the factorization formula eq. (2.12). Here Q is the hard scale, λ is the small expansion parameter $\lambda \equiv p_T^{\rm cut}/Q \ll 1$, while R_J is the radius of the signal jet $R_J \ll 1$. Where applicable, the collinear direction associated to each mode as specified in eq. (2.10) is given in parentheses.

$$|y_H - Y| \leq \operatorname{arccosh}\left(\frac{e^{-|Y|}(E_{\rm cm}^2 + e^{2|Y|}m_H^2)}{2E_{\rm cm}\, E_T^H}\right). \tag{2.9}$$

2.2 Factorization formula

In this section we detail the effective field theory and factorization formula used to describe $pp \to H{+}1$ jet in the presence of a jet veto. The veto is implemented by requiring additional jets to have transverse momentum $p_T < p_T^{\rm cut}$. We define our jets using the anti-k_T clustering algorithm. We distinguish between the jet radius of the signal jet R_J and that of vetoed jets $R_{\rm cut}$ to elucidate how each enters into our calculation. The typical experimental ranges of the jet-p_T veto are $p_T^{\rm cut} \sim 25 - 30\,\text{GeV}$, meaning that we consider the hierarchy $p_T^{\rm cut} \ll Q$ and the resummation of logarithms of $p_T^{\rm cut}/Q$ (where Q is defined in eq. (2.3)). We also work in the narrow-jet limit, $R_J, R_{\rm cut} \ll 1$. The limit $R_J \ll 1$ is necessary to factorize the signal jet as we will see momentarily. As discussed in ref. [14], the condition $R_{\rm cut} \ll 1$ is needed to derive a valid all-order factorization formula in the presence of the jet-veto measurement. We focus on the regime in which the signal jet is hard, $p_T^J \sim m_H \sim Q$, and well-separated in rapidity from the beam directions. In this way we are able to avoid introducing additional scale hierarchies into the problem.

Having identified our expansion parameters $\lambda \equiv p_T^{\rm cut}/Q \ll 1$ and $R_J, R_{\rm cut} \ll 1$, the next step is to establish the relevant degrees of freedom or modes in Soft-Collinear Effective Theory (SCET) [43–47]. To this end, we introduce three light-like reference vectors n_a, n_b, and n_J for the three collinear directions associated with the three hard partons, as well as conjugate vectors $\bar{n}_a$, $\bar{n}_b$, and $\bar{n}_J$,

$$\begin{aligned} n_a^\mu &= (1,0,0,1), \qquad & n_b^\mu &= (1,0,0,-1), \qquad & n_J^\mu &= (\cosh y_J, 1, 0, \sinh y_J)\,, \\ \bar{n}_a^\mu &= (1,0,0,-1), \qquad & \bar{n}_b^\mu &= (1,0,0,1), \qquad & \bar{n}_J^\mu &= (\cosh y_J, -1, 0, -\sinh y_J)\,, \end{aligned} \tag{2.10}$$

where we choose as usual the beam direction to be the z axis and the normalization $n_i \cdot \bar{n}_i = 2$. Any four-momentum can then be decomposed into components along the light-cone vectors n_i^μ and $\bar{n}_i^\mu$, and the components transverse to these $p_{\perp i}^\mu$,

$$p^\mu = p^+ \frac{\bar{n}_i^\mu}{2} + p^- \frac{n_i^\mu}{2} + p_{\perp i}^\mu \qquad p^+ = n_i \cdot p\,, \qquad p^- = \bar{n}_i \cdot p\,. \tag{2.11}$$

Expressed in terms of these reference vectors, the requirement that the signal jet is well-separated in rapidity from the beam directions is given by $n_a \cdot n_J \sim n_b \cdot n_J \sim 1$.

JHEP03(2025)155

We now describe the various modes in SCET, which are summarized in table 1. There are collinear modes associated with the beams and jet, which carry the large momentum flowing in these directions. The power counting of these modes is most naturally expressed in the corresponding light-cone coordinates. The jet-veto measurement sets the power counting for the transverse momentum of collinear radiation along the beams. Due to its large energy, the jet collinear radiation must be confined to the jet, so its transverse momentum *with respect to the jet axis* should be of order $p_T^J R_J$. The typical virtuality scale of collinear emissions describing the jet is thus $p_T^J R_J \sim Q R_J$, which for the factorization to hold must be parametrically smaller than the hard scale Q. This is why we have to require $R_J \ll 1$. The wide-angle soft radiation does not resolve the small angular scale R_J of the jet and the jet veto sets its transverse momentum to be of order p_T^{cut}. It is isotropic and so independent of which light-cone coordinates are used. Finally, there is soft-collinear radiation, whose power counting is set by the requirement that it resolves the jet, i.e. its typical angular scale is R_J, and which is sensitive to the jet veto measurement, so that its energy is of order p_T^{cut}. Hence, having to require $R_J \ll 1$ inevitably leads to the appearance of the additional soft-collinear scale $p_T^{\text{cut}} R_J$ with the same parametric distinction from the soft scale p_T^{cut} as that between the jet and hard scales.

This mode picture leads to the following form of the factorized cross section:

$$\begin{aligned}\frac{\mathrm{d}\sigma}{\mathrm{d}p_T^J \mathrm{d}Y \,\mathrm{d}y_J}(p_T^{\text{cut}}) = \sum_\kappa H_\kappa(p_T^J, Y, y_J; \mu) B_a\Big(p_T^{\text{cut}}, x_a, R_{\text{cut}}; \mu, \frac{\nu}{\omega_a}\Big)\, B_b\Big(p_T^{\text{cut}}, x_b, R_{\text{cut}}; \mu, \frac{\nu}{\omega_b}\Big) \\ \times J_j(p_T^J R_J; \mu)\, S_\kappa(p_T^{\text{cut}}, R_{\text{cut}}, y_J; \mu, \nu)\, \mathcal{S}_j^R(p_T^{\text{cut}} R_J; \mu)\, \mathcal{S}_j^{\text{NG}}\Big(\frac{p_T^{\text{cut}}}{p_T^J}\Big) \\ \times \Big[1 + \mathcal{O}\Big(\frac{p_T^{\text{cut}}}{Q}, R_{\text{cut}}^2, R_J^2\Big)\Big]. \end{aligned} \tag{2.12}$$

The sum over $\kappa = \{a, b, j\}$ runs over the possible flavours $a, b, j \in \{g, u, \bar{u}, \dots\}$ of the incoming and outgoing partons. H_κ denotes the hard function, which encodes the hard scattering process $ab \to Hj$ (and though written as a function of both Y and y_J, depends only on the Lorentz-invariant difference $Y - y_J$). The beam functions B describe initial-state collinear radiation from the incoming partons (with x_i and ω_i defined in eq. (2.4)), while the global soft function S describes isotropic soft radiation. Hard-collinear radiation along the jet direction is described by the jet function J.

The soft-collinear function $\mathcal{S}_j^R$ is associated with the soft-collinear mode described above. Such soft-collinear modes were introduced in a similar context in ref. [48] to resum the logarithms of R_J in the soft sector, which arise from the ratio of the soft and soft-collinear scales p_T^{cut} and $p_T^{\text{cut}} R_J$. These are distinct in origin from logarithms of R_J arising from the ratio of the hard and jet scales p_T^J and $p_T^J R_J$, whose resummation is addressed by the factorization between the jet and hard function. While we are able to resum all logarithms of R_J, there are logarithms of R_{cut} which remain unresummed (as discussed in ref. [14]). For work on these clustering logarithms beyond their contribution to the NNLO cross section, see refs. [18, 42, 49]. Finally, since the in-jet region is unconstrained and the out-of-jet region is sensitive to the p_T-veto measurement, there are nonglobal logarithms (NGLs) of p_T^{cut}/p_T^J, arising from the separation of the soft-collinear and n_J-collinear modes [50, 51]. As

JHEP03(2025)155

discussed in section 3.1.4, we will include the leading nonglobal logarithms in the function $\mathcal{S}_j^{\mathrm{NG}}$, which formally contribute at NLL order to the cross section but which are in practice numerically small.

Before moving on to a detailed analysis of the validity of the factorization in eq. (2.12), it is worth commenting on the differences with respect to the work of ref. [36] where the resummation of veto logarithms for $pp \to H{+}1$ jet was originally studied. The main difference between the factorization formula presented in that work and eq. (2.12) is the additional refactorization of the soft sector into global soft, soft-collinear and nonglobal pieces. Compared to ref. [36] which treated only logarithms of R_J arising from the ratio of the jet and hard scales, this allows us also to deal with equally large logarithms of the ratio of soft and soft-collinear scales. Having supplemented this with the resummation of the leading nonglobal logarithms and the inclusion in the soft sector of subleading terms in R_J (see section 3.2), we have been able to address many of the issues identified by the authors of ref. [36] as topics for future study.

2.3 Factorization analysis

The all-order validity of the leading-power factorization formula in eq. (2.12) rests on the factorization properties of the measurement, which we will now discuss in some detail. The measurement function acting on the complete final state is given by

$$\mathcal{M}(p_T^{\mathrm{cut}}, R_{\mathrm{cut}}, R_J) = \prod_{j \in \mathcal{J}(R_{\mathrm{cut}}, R_J)} \Theta(|\vec{p}_{Tj}| < p_T^{\mathrm{cut}}) \,, \tag{2.13}$$

where $\mathcal{J}(R_{\mathrm{cut}}, R_J)$ denotes the set of all additional jets beyond the signal jet. More precisely, we first run the jet algorithm with R_J to identify the leading signal jet and remove all its particles from the final state. We then run the jet algorithm again with R_{cut} on this reduced final state and denote its outcome by $\mathcal{J}(R_{\mathrm{cut}}, R_J)$. To establish eq. (2.12), we must be able to separate the full measurement in eq. (2.13) into a product of measurements acting independently on the soft, beam-collinear, jet-collinear, and soft-collinear sectors. That is, we wish to make the decomposition

$$\mathcal{M} = \mathcal{M}_a \, \mathcal{M}_b \, \mathcal{M}_J \, \mathcal{M}_s \, \mathcal{M}_{sc} + \delta\mathcal{M} \,, \tag{2.14}$$

where the measurement applied independently within each individual sector is denoted by $\mathcal{M}_i$, implicitly defining a remainder term $\delta\mathcal{M}(p_T^{\mathrm{cut}})$. Achieving factorization amounts to demonstrating that this remainder function (more precisely its contribution to the cross section) is power-suppressed, or in other words that the measurement does not mix or entangle the constraints on different sectors to leading power.[2] Assuming the jet algorithm does not cluster emissions from different sectors, the product form in eq. (2.14) immediately follows from the product of Θ functions in eq. (2.13) with $\delta\mathcal{M} = 0$ [14].

In ref. [14], the properties of jet-veto resummations were studied for the class of processes $pp \to V$, where V represents any colour-singlet final state. It was shown that the contribution

[2] To be precise, the measurement entangling the constraints on individual emissions in different sectors does not necessarily preclude any resummation. It does prevent a simple (in our case multiplicative) all-order factorization structure of the cross section, from which the resummation to any resummation order would follow.

JHEP03(2025)155

from mixing of soft and $n_{a,b}$-collinear sectors entering in $\delta\mathcal{M}(p_T^{\text{cut}})$ is indeed power-suppressed by $\mathcal{O}(R_{\text{cut}}^2)$.[3] It remains for us to demonstrate that the additional n_J-collinear and soft-collinear sectors in our case do not yield any further, unsuppressed mixing terms.

Firstly, $n_{a,b}$-collinear and n_J-collinear particles cannot be clustered at leading power, just as the clustering of n_a-collinear and n_b-collinear particles is not allowed. Next, we consider the case in which a n_J-collinear particle is clustered with a soft particle. This is power suppressed by $\mathcal{O}(R_J^2)$ for the global soft sector, since it describes wide-angle radiation and does not resolve the jet boundary. Soft-collinear radiation, however, does resolve the jet boundary. This can in principle lead to clustering effects — in appendix A, we demonstrate that these contribute at the same level as subleading nonglobal logarithms. Since we include only the leading nonglobal terms in this work (see section 3.1.5), we can thus use a static boundary in calculating the soft-collinear function and ignore the effect of clustering with individual n_J-collinear emissions. At this point, we can conclude that the full measurement factorizes as

$$\begin{aligned}\mathcal{M}(p_T^{\text{cut}}, R_{\text{cut}}, R_J) = \mathcal{M}_a(p_T^{\text{cut}}, R_{\text{cut}})\mathcal{M}_b(p_T^{\text{cut}}, R_{\text{cut}})\mathcal{M}_J(R_J)\mathcal{M}_{\text{soft}}(p_T^{\text{cut}}, R_{\text{cut}}, R_J) \\ \times \left[1 + \mathcal{O}(R_J^2, R_{\text{cut}}^2)\right].\end{aligned} \tag{2.15}$$

where

$$\mathcal{M}_{a,b}(p_T^{\text{cut}}, R_{\text{cut}}) = \prod_{j \in \mathcal{J}_{a,b}(R_{\text{cut}})} \Theta(|\vec{p}_{Tj}| < p_T^{\text{cut}}). \tag{2.16}$$

is the standard jet-veto measurement in the $n_{a,b}$-collinear sectors with $\mathcal{J}_{a,b}(R_{\text{cut}})$ denoting the set of all jets returned by the jet algorithm acting solely on the $n_{a,b}$-collinear final state. In particular, for the same reason $n_{a,b}$-collinear emissions cannot be clustered with n_J-collinear ones, the $\mathcal{M}_{a,b}$ do not depend at all on the presence of the signal jet and R_J.

The n_J-collinear measurement $\mathcal{M}_J(R_J)$ simply constrains all n_J-collinear emissions to lie inside the signal jet without any further constraints inside the jet.[4] In particular, it does not actually depend on the jet-veto measurement and p_T^{cut}. To see this, assume there is an n_J-collinear emission outside the signal jet. It would be clustered into its own jet with $p_T \sim p_T^J$, which would then be subject to the jet-veto requirement $p_T^J < p_T^{\text{cut}}$, which however violates the power counting $p_T^{\text{cut}} \ll p_T^J$. Hence, the jet veto outside the signal jet effectively forces all n_J-collinear emissions to be clustered into the signal jet.

The last measurement in eq. (2.15) is given by

$$\mathcal{M}_{\text{soft}}(p_T^{\text{cut}}, R_J, R_{\text{cut}}) = \prod_{j \in \mathcal{J}_{\text{soft}}(R_{\text{cut}}, R_J)} \Theta(|\vec{p}_{Tj}| < p_T^{\text{cut}}). \tag{2.17}$$

It acts on the total soft sector comprised of both soft and soft-collinear emissions, where $\mathcal{J}_{\text{soft}}(R_{\text{cut}}, R_J)$ denotes the result of the jet algorithm acting on both soft and soft-collinear

[3] As discussed in detail in ref. [14], due to the presence of such mixing in the measurement function the all-order factorization and resummation at $\mathcal{O}(R_{\text{cut}}^2)$ is presently unknown, since the standard leading-power arguments become insufficient at $\mathcal{O}(R_{\text{cut}}^2)$. The mixing contributions first appear at fixed $\mathcal{O}(\alpha_s^2)$. There are different schemes to incorporate them into the final resummed result [15–17], which are formally equivalent at NNLL as discussed in detail in ref. [52].

[4] This means that, in the terminology of ref. [53], we are considering an unmeasured jet function. The relationship between measured and unmeasured jet functions is further discussed in ref. [48].

JHEP03(2025)155

emissions outside a fixed cone of R_J around the jet direction n_J. The remaining step is to consider the factorization of

$$\mathcal{M}_{\rm soft}(p_T^{\rm cut}, R_{\rm cut}, R_J) = \mathcal{M}_s(p_T^{\rm cut}, R_{\rm cut})\, \mathcal{M}_{sc}(p_T^{\rm cut}, R_{\rm cut}, R_J) \tag{2.18}$$

into measurements acting separately on the global (i.e. overall) soft and the soft-collinear sectors, and in the process determine the precise form of the soft-collinear measurement function $\mathcal{M}_{sc}$. With no particles in the final state, we trivially have

$$\mathcal{M}_{\rm soft}^{[0]} = 1 = 1 \times 1 \equiv \mathcal{M}_s^{[0]} \mathcal{M}_{sc}^{[0]}\,, \tag{2.19}$$

where the superscript $[n]$ denotes the measurement acting on the n-particle final state. This result corresponds to $S^{(0)}\mathcal{S}^{R,(0)}$.

For a single emission,

$$\begin{aligned}\mathcal{M}_{\rm soft}^{[1]} &= \mathbf{1}_{\rm in} + \mathbf{1}_{\rm out}\mathbf{1}_{\rm cut} = \mathbf{1}_{\rm in}(\mathbf{1}_{\rm cut} + \bar{\mathbf{1}}_{\rm cut}) + \mathbf{1}_{\rm out}\mathbf{1}_{\rm cut} \\ &= \underbrace{\mathbf{1}_{\rm cut}}_{\mathcal{M}_s^{[1]}} + \underbrace{\mathbf{1}_{\rm in}\bar{\mathbf{1}}_{\rm cut}}_{\mathcal{M}_{sc}^{[1]}} \equiv \mathcal{M}_s^{[1]}\mathcal{M}_{sc}^{[0]} + \mathcal{M}_s^{[0]}\mathcal{M}_{sc}^{[1]} = (\mathcal{M}_s\mathcal{M}_{sc})^{[1]}\,,\end{aligned} \tag{2.20}$$

where $\mathbf{1}_{\rm in}$ and $\mathbf{1}_{\rm out}$ denote the restriction (i.e. a suitable set of theta functions) for particle 1 to be inside and outside the signal jet respectively. Similarly, $\mathbf{1}_{\rm cut}$ denotes the restriction that the p_T of particle 1 is below $p_T^{\rm cut}$. The bar denotes the complement of a restriction, e.g. $\mathbf{1}_{\rm out} = \bar{\mathbf{1}}_{\rm in} = 1 - \mathbf{1}_{\rm in}$. The first equality simply encodes the full measurement on the soft emission, namely that its p_T is constrained when outside the jet and unconstrained when inside the jet, which can be rewritten as shown. In the second line we can identify the measurement $\mathcal{M}_s^{[1]}$ acting on the global soft radiation, which does not resolve the jet and therefore the emission is constrained by $p_T^{\rm cut}$ everywhere. The form of the soft-collinear measurement $\mathcal{M}_{sc}^{[1]} = \mathbf{1}_{\rm in}\bar{\mathbf{1}}_{\rm cut}$ is perhaps not intuitive. It can be interpreted as correcting the global soft measurement inside the jet by adding back the soft emissions that are removed by the global soft measurement, or equivalently as $\mathcal{M}_{sc}^{[1]} = \mathbf{1}_{\rm in} - \mathbf{1}_{\rm in}\mathbf{1}_{\rm cut}$ as subtracting the overlap with the global soft measurement to avoid double counting.

Next, for two soft emissions we have

$$\begin{aligned}\mathcal{M}_{\rm soft}^{[2]} &= \mathbf{1}_{\rm in}\mathbf{2}_{\rm in} + \mathbf{1}_{\rm in}\mathbf{2}_{\rm out}\mathbf{2}_{\rm cut} + \mathbf{1}_{\rm out}\mathbf{1}_{\rm cut}\mathbf{2}_{\rm in} + \mathbf{1}_{\rm out}\mathbf{2}_{\rm out}(\{\mathbf{12}\}_{\rm clust}\{\mathbf{12}\}_{\rm cut} + \overline{\{\mathbf{12}\}}_{\rm clust}\mathbf{1}_{\rm cut}\mathbf{2}_{\rm cut}) \\ &= \underbrace{(\mathbf{1}_{\rm cut} + \mathbf{1}_{\rm in}\bar{\mathbf{1}}_{\rm cut})(\mathbf{2}_{\rm cut} + \mathbf{2}_{\rm in}\bar{\mathbf{2}}_{\rm cut})}_{\mathcal{M}_{\rm soft,no\ clust}^{[2]}} + \underbrace{\mathbf{1}_{\rm out}\mathbf{2}_{\rm out}\{\mathbf{12}\}_{\rm clust}(\{\mathbf{12}\}_{\rm cut} - \mathbf{1}_{\rm cut}\mathbf{2}_{\rm cut})}_{\mathcal{M}_{\rm soft,clust}^{[2]}}\end{aligned} \tag{2.21}$$

where $\{\mathbf{12}\}_{\rm clust}$ encodes the condition that particle 1 and 2 are clustered and $\{\mathbf{12}\}_{\rm cut}$ denotes the p_T cut on their combined momenta. In the first term, $\mathcal{M}_{\rm soft,no\ clust}^{[2]}$, no clustering happens so each emission is treated as its own jet. It is clear that these contributions factorize, being of the form

$$\mathcal{M}_{\rm soft,no\ clust}^{[2]} \equiv \left(\mathcal{M}_s^{[2]} + \mathcal{M}_s^{[1]}\mathcal{M}_{sc}^{[1]} + \mathcal{M}_{sc}^{[2]}\right)_{\rm no\ clust} = (\mathcal{M}_s\mathcal{M}_{sc})^{[2]}_{\rm no\ clust}\,. \tag{2.22}$$

Note that when written as a product of separate measurement operators acting on separate sectors in the final state, the product $\mathcal{M}_s^{[1]}\mathcal{M}_{sc}^{[1]}$ accounts for both cross terms $\mathbf{1}_{\rm cut}\mathbf{2}_{\rm in}\bar{\mathbf{2}}_{\rm cut}$

JHEP03(2025)155

and $\mathbf{2}_{\rm cut}\mathbf{1}_{\rm in}\bar{\mathbf{1}}_{\rm cut}$ appearing in eq. (2.21), depending on which of the final-state particles is soft or soft-collinear.

The second term in eq. (2.21), $\mathcal{M}^{[2]}_{\rm soft,clust}$, contains the clustering correction, which we can rewrite as

$$\mathcal{M}^{[2]}_{\rm soft,clust} = \underbrace{\{\mathbf{12}\}_{\rm clust}(\{\mathbf{12}\}_{\rm cut} - \mathbf{1}_{\rm cut}\mathbf{2}_{\rm cut})}_{\mathcal{M}^{[2]}_{s,\rm clust}} + \underbrace{(\mathbf{1}_{\rm out}\mathbf{2}_{\rm out} - 1)\{\mathbf{12}\}_{\rm clust}(\{\mathbf{12}\}_{\rm cut} - \mathbf{1}_{\rm cut}\mathbf{2}_{\rm cut})}_{\mathcal{M}^{[2]}_{sc,\rm clust}} . \tag{2.23}$$

$\mathcal{M}^{[2]}_{s,\rm clust}$ corresponds to the global soft contribution, which does not involve the jet boundary, and $\mathcal{M}^{[2]}_{sc,\rm clust}$ is defined by the difference between $\mathcal{M}^{[2]}_{\rm soft,clust}$ and $\mathcal{M}^{[2]}_{s,\rm clust}$. We can now argue that $\mathcal{M}^{[2]}_{sc,\rm clust}$ is fully accounted for by the soft-collinear function, because the constraint $(\mathbf{1}_{\rm out}\mathbf{2}_{\rm out} - 1)$ forces at least one of the two emissions to be inside the jet, whilst the clustering condition $\{\mathbf{12}\}_{\rm clust}$ forces the other emission to have separation $R_{\rm cut}$ to it. Hence, for the case $R_{\rm cut} \sim R_J \ll 1$ that we consider, both emissions are forced to have the same angular scale and thus belong to the soft-collinear sector.[5] Combining the two contributions we have

$$\mathcal{M}^{[2]}_{\rm soft} = (\mathcal{M}_s\mathcal{M}_{sc})^{[2]}_{\text{no clust}} + \mathcal{M}^{[2]}_{s,\rm clust} + \mathcal{M}^{[2]}_{sc,\rm clust} = (\mathcal{M}_s\mathcal{M}_{sc})^{[2]} . \tag{2.24}$$

It should be clear that the above pattern extends to any number of soft emissions. First, without any clustering, we immediately have

$$\mathcal{M}^{[n]}_{\text{soft,no clust}} = \prod_{\mathbf{k=1}}^{\mathbf{n}} (\mathbf{k}_{\rm cut} + \mathbf{k}_{\rm in}\bar{\mathbf{k}}_{\rm cut}) = (\mathcal{M}_s\mathcal{M}_{sc})^{[n]}_{\text{no clust}} . \tag{2.25}$$

Including clustering effects, we define the soft measurement as the jet-veto measurement acting on the soft sector without any reference to the signal jet,

$$\mathcal{M}_s(p_T^{\rm cut}, R_{\rm cut}) = \prod_{j\in\mathcal{J}_s(R_{\rm cut})} \Theta(|\vec{p}_{Tj}| < p_T^{\rm cut}) , \tag{2.26}$$

where $\mathcal{J}_s(R_{\rm cut})$ is the result of the jet algorithm acting on the soft final state. The resulting soft function by definition only depends on the scale $p_T^{\rm cut}$ but not on R_J. Starting at $\mathcal{O}(\alpha_s^2)$, it will also include clustering logarithms of $R_{\rm cut}$, which here we do not aim to resum but include at fixed order, as discussed earlier.

The soft-collinear measurement is then defined for any number of emissions as the necessary correction with respect to the full measurement including all clustering effects. That is, we use eq. (2.18) to solve for $\mathcal{M}_{sc}$ with $\mathcal{M}_{\rm soft}$ and $\mathcal{M}_s$ given in eqs. (2.17) and (2.26), analogous to what we did for one and two emissions above. Symbolically, we can write

$$\mathcal{M}_{sc}(p_T^{\rm cut}, R_{\rm cut}, R_J) = \mathcal{M}_{\rm soft}(p_T^{\rm cut}, R_{\rm cut}, R_J)\mathcal{M}_s^{-1}(p_T^{\rm cut}, R_{\rm cut}) . \tag{2.27}$$

The last step is to argue that this remaining constraint indeed forces all involved emissions to be soft-collinear, i.e., to have the same small angular scale given by $R_J \sim R_{\rm cut}$, analogous to

[5] On the other hand, in case of a hierarchy $R_J \ll R_{\rm cut} \sim 1$, one of the emissions could be a wide-angle soft emission outside the jet, implying a mixing between the soft and soft-collinear measurement constraints, which would prevent us from establishing a simple (multiplicative) measurement factorization using only power-counting arguments.

JHEP03(2025)155

what we found for $\mathcal{M}^{[2]}_{sc,\text{clust}}$ in case of two emissions above. First, we can always rewrite the total soft measurement including clustering for n emissions analogously to the second line of eq. (2.21) as the no-clustering contribution eq. (2.25) plus a clustering correction, which in general is a sum of products of clustering constraints of the form

$$\mathbf{1}_{\text{out}}\mathbf{2}_{\text{out}}\cdots\mathbf{k}_{\text{out}}\{\mathbf{12}\cdots\mathbf{k}\}_{\text{clust}}(\dots) \equiv \{\mathbf{k}\}_{\text{out}}\{\mathbf{k}\}_{\text{clust}}(\cdots)\,, \tag{2.28}$$

where k particles are clustered together in a jet and the parantheses only contain differences of p_T^{cut} constraints to appropriately correct from the unclustered to the clustered case. In particular, since the jet algorithm for $\mathcal{M}_{\text{soft}}$ only acts outside the signal jet any clustering correction for k particles must have the constraint $\{\mathbf{k}\}_{\text{out}} = \mathbf{1}_{\text{out}}\cdots\mathbf{k}_{\text{out}}$ as shown, forcing all particles to be outside the jet. The global soft measurement can be written in exactly the same way, except that this constrain is absent. For a single clustering term like the above, the resulting remainder appearing in $\mathcal{M}^{[k]}_{sc}$ is then given by

$$\underbrace{(\{\mathbf{k}\}_{\text{out}}-1)\{\mathbf{k}\}_{\text{clust}}(\dots)}_{\in\mathcal{M}^{[k]}_{\text{sc,clust}}} = \underbrace{\{\mathbf{k}\}_{\text{out}}\{\mathbf{k}\}_{\text{clust}}(\dots)}_{\in\mathcal{M}^{[k]}_{\text{soft,clust}}} - \underbrace{\{\mathbf{k}\}_{\text{clust}}(\dots)}_{\in\mathcal{M}^{[k]}_{\text{s,clust}}}\,, \tag{2.29}$$

which forces all involved k emissions to be soft-collinear because it requires at least one of the emissions to be inside the signal jet and all others to be clustered with it. For a product of such clustering terms, say for k_i and k_j particles that are clustered into separate jets, their constraints to be outside the signal jet can always be rearranged as

$$\begin{aligned}\underbrace{\{\mathbf{k_i}\}_{\text{out}}\{\mathbf{k_j}\}_{\text{out}}}_{\in\mathcal{M}^{[k_i+k_j]}_{\text{soft,clust}}} &= (\{\mathbf{k_i}\}_{\text{out}}-1+1)(\{\mathbf{k_j}\}_{\text{out}}-1+1) \\ &= \underbrace{(\{\mathbf{k_i}\}_{\text{out}}-1)(\{\mathbf{k_j}\}_{\text{out}}-1)}_{\in\mathcal{M}^{[k_i+k_j]}_{sc,\text{clust}}} + \underbrace{(\{\mathbf{k_i}\}_{\text{out}}-1)\times 1}_{\in\mathcal{M}^{[k_i]}_{sc,\text{clust}}\mathcal{M}^{[k_j]}_{\text{s,clust}}} + \underbrace{1\times(\{\mathbf{k_j}\}_{\text{out}}-1)}_{\in\mathcal{M}^{[k_i]}_{\text{s,clust}}\mathcal{M}^{[k_j]}_{sc,\text{clust}}} + \underbrace{1}_{\in\mathcal{M}^{[k_i+k_j]}_{\text{s,clust}}}\,,\end{aligned} \tag{2.30}$$

where for brevity we have dropped the overall factor of $\{\mathbf{k_i}\}_{\text{clust}}\{\mathbf{k_j}\}_{\text{clust}}$ on both sides. The first term on the right-hand side again forces both sets of particles to be soft-collinear. As indicated, the cross terms correspond to cross terms in $[\mathcal{M}_s\mathcal{M}_{sc}]^{[k_i+k_j]}_{\text{clust}}$. Finally, whenever clustering terms appear multiplied by additional unclustered emissions, these are accounted for by cross terms between lower-emission clustering and no-clustering contributions.

It may not be obvious where the nonglobal logarithms, included through $\mathcal{S}^{\text{NG}}$ in eq. (2.12), appear in this discussion. These leading nonglobal logarithms arise from the soft-collinear sector i.e., the matrix element of $\mathcal{M}_{sc}$ gives rise to the product $\mathcal{S}_j^R\mathcal{S}_j^{\text{NG}}$ in eq. (2.12). Specifically, they are not caused by a failure of the measurement to factorize, but are due to correlated soft-collinear emissions involving both the constrained and unconstrained regions of phase space. In practice, the jet scale p_T^J limits the radiation in the unconstrained region, leading to nonglobal logarithms of p_T^J/p_T^{cut}. Subleading nonglobal logarithms are sensitive to collinear emissions inside the jet — their resummation is more complicated, and cannot be achieved using a factorisation formula of the kind studied in this work. Resummation has nevertheless been achieved up to NLL using both coherent branching and SCET approaches [54, 55]. At the same order the effect of soft-collinear clustering also enters, described in appendix A.

JHEP03(2025)155

3 Resummation at NNLL′+NNLO

We begin this section by presenting the necessary perturbative ingredients in section 3.1. We use these to validate the singular structure of the cross section at next-to-leading order in section 3.2. This validation reveals relatively large power corrections in the jet radius, arising from the factorization of the total soft function into a global and soft-collinear part (discussed in section 3.1.4). The resummation is discussed in section 3.3, and the treatment of the missing ingredients needed to reach (global) NNLL′ accuracy using theory nuisance parameters (TNPs) is presented in section 3.4.

3.1 Perturbative ingredients

In this section we provide (most of) the perturbative ingredients necessary to attain (global) NNLL′ accuracy. We will express these in terms of the cusp and noncusp anomalous dimensions, using the following convention for their expansion in α_s:

$$\Gamma^i_{\text{cusp}}(\alpha_s) = \sum_{n=0}^{\infty} \Gamma^i_n \Big(\frac{\alpha_s}{4\pi}\Big)^{n+1}, \qquad \gamma^i_F(\alpha_s) = \sum_{n=0}^{\infty} \gamma^i_{F\,n} \Big(\frac{\alpha_s}{4\pi}\Big)^{n+1}. \tag{3.1}$$

Here F stands for any function in the factorized cross section in eq. (2.12), i.e. hard, beam, soft, soft-collinear or jet function, and γ_F its noncusp anomalous dimension. The superscript $i \in \{q, g\}$ specifies the representation of the colour algebra. It will occasionally be convenient to use the colour-stripped coefficients of the cusp anomalous dimension $\Gamma_n = \Gamma^i_n/C_i$ for $n \leq 2$, with the overall colour factor $C_i = C_A$ (C_F) for $i = g$ ($i = q$) made explicit. Similarly, the β-function is expanded as

$$\beta(\alpha_s) = -2\alpha_s \sum_{n=0}^{\infty} \beta_n \Big(\frac{\alpha_s}{4\pi}\Big)^{n+1}. \tag{3.2}$$

The coefficients in eqs. (3.1) and (3.2) needed up to NNLL′ are given in eqs. (C.3) and (C.4). The boundary condition for a function F in the factorized cross section is expanded as

$$F = \sum_{n=0}^{\infty} \Big(\frac{\alpha_s}{4\pi}\Big)^n F^{(n)}. \tag{3.3}$$

3.1.1 Hard function

We work in the heavy-top limit in which the top-quark loop coupling the Higgs boson to gluons has been integrated out, resulting in the effective Lagrangian

$$\mathcal{L}_{\text{eff}} = C_t \frac{\alpha_s}{12\pi} \frac{H}{v} G^a_{\mu\nu} G^{a\,\mu\nu}, \tag{3.4}$$

where the Wilson coefficient C_t has an expansion in α_s. In this limit, the relevant hard functions can be extracted from the helicity amplitudes [56, 57], which were computed at 1-loop order in ref. [58] and at 2-loops in ref. [59]. The squared amplitudes can be written as

$$\begin{aligned}
|\mathcal{M}^{+++}_{ggg}(p_1, p_2, p_3)|^2 &= \frac{M_H^8}{2\varsigma_{12}\varsigma_{23}\varsigma_{13}} |\alpha|^2, \\
|\mathcal{M}^{++-}_{ggg}(p_1, p_2, p_3)|^2 &= \frac{\varsigma_{12}^3}{2\varsigma_{23}\varsigma_{13}} |\beta|^2, \\
|\mathcal{M}^{-++}_{q\bar{q}g}(p_1, p_2, p_3)|^2 &= \frac{\varsigma_{23}^2}{2\varsigma_{12}} |\gamma|^2,
\end{aligned} \tag{3.5}$$

JHEP03(2025)155

where $\varsigma_{ij} = 2p_i \cdot p_j$ and the functions α, β and γ admit a perturbative expansion in $\alpha_s(\mu)$.[6] The remaining helicity amplitudes can be deduced by exploiting parity and charge conjugation symmetries. We are interested in the case in which the momenta $p_1 = p_a$ and $p_2 = p_b$ are incoming and $p_3 = p_J$ is outgoing. Using the definitions in eq. (2.2) and further defining

$$t = \frac{s_{aJ}}{s_{ab}}\,, \qquad u = \frac{s_{bJ}}{s_{ab}}\,, \qquad v = \frac{M_H^2}{s_{ab}}\,, \tag{3.6}$$

the hard functions can be written as

$$\begin{aligned}
H_{ggg}(s_{ab}, s_{bJ}, s_{aJ}) &= 2\bigg[\frac{M_H^8}{2s_{ab}s_{bJ}s_{aJ}}|\alpha_2(t,v)|^2 + \frac{s_{ab}^3}{2s_{bJ}s_{aJ}}|\beta_2(t,v)|^2 \\
&\qquad + \frac{s_{bJ}^3}{2s_{ab}s_{aJ}}|\beta_4(t,v)|^2 + \frac{s_{aJ}^3}{2s_{ab}s_{bJ}}|\beta_4(u,v)|^2\bigg], \\
H_{q\bar{q}g}(s_{ab}, s_{bJ}, s_{aJ}) &= 2\bigg[\frac{s_{bJ}^2}{2s_{ab}}|\gamma_2(u,v)|^2 + \frac{s_{aJ}^2}{2s_{ab}}|\gamma_2(t,v)|^2\bigg], \\
H_{qgq}(s_{ab}, s_{bJ}, s_{aJ}) &= 2\bigg[\frac{s_{bJ}^2}{2s_{aJ}}|\gamma_3(u,v)|^2 + \frac{s_{ab}^2}{2s_{aJ}}|\gamma_4(u,v)|^2\bigg]\,,
\end{aligned} \tag{3.7}$$

where the subscript $n = \{2, 3, 4\}$ on the functions α, β, γ denotes the kinematic region in which they are to be evaluated, following the conventions of ref. [56]. We take the perturbative coefficients of these functions from that reference, where the translation from the Catani scheme in which they were originally computed to the $\overline{\text{MS}}$ scheme conventionally used in SCET has already been performed.[7] Since their expressions, even at one loop, are rather involved, we refrain from writing them out explicitly here.

Lastly, the renormalization group equation (RGE) for the hard function is given by

$$\mu\frac{\mathrm{d}}{\mathrm{d}\mu}\ln H_\kappa(p_T^J, Y, y_J; \mu) = \gamma_H^\kappa(p_T^J, Y, y_J; \mu) \tag{3.8}$$

where the hard anomalous dimension is given to all orders by [60]

$$\gamma_H^\kappa(s_{ab}, s_{aJ}, s_{bJ}; \mu) = \sum_{(klm)} \Big\{\Gamma_{\text{cusp}}^m[\alpha_s(\mu)] - \Gamma_{\text{cusp}}^k[\alpha_s(\mu)] - \Gamma_{\text{cusp}}^l[\alpha_s(\mu)]\Big\}\ln\frac{|s_{kl}|}{\mu^2} + \gamma_H^\kappa[\alpha_s(\mu)]\,, \tag{3.9}$$

where the sum runs over the three permutations $(klm) = (abJ), (aJb), (bJa)$. Up to two loops the noncusp anomalous dimension is given by

$$\begin{aligned}
\gamma_H^\kappa(\alpha_s) &= 2\gamma_C^a(\alpha_s) + 2\gamma_C^b(\alpha_s) + 2\gamma_C^j(\alpha_s) + \mathcal{O}(\alpha_s^3)\,, \\
\gamma_{C\,0}^q &= -3C_F\,, \\
\gamma_{C\,1}^q &= -C_F\bigg[C_A\Big(\frac{41}{9} - 26\zeta_3\Big) + C_F\Big(\frac{3}{2} - 2\pi^2 + 24\zeta_3\Big) + \beta_0\Big(\frac{65}{18} + \frac{\pi^2}{2}\Big)\bigg]\,, \\
\gamma_{C\,0}^g &= -\beta_0\,, \\
\gamma_{C\,1}^g &= C_A\bigg[C_A\Big(-\frac{59}{9} + 2\zeta_3\Big) + \beta_0\Big(-\frac{19}{9} + \frac{\pi^2}{6}\Big)\bigg] - \beta_1\,.
\end{aligned} \tag{3.10}$$

[6] In the following we will suppress the μ dependence in our notation.

[7] We note that the original results for the $q\bar{q} \to Hg$ channel presented in ref. [59] contained a typographical error in the ancillary files. This was remedied in the later results of ref. [56].

JHEP03(2025)155

3.1.2 Jet function

The jet function RGE is given by

$$\mu \frac{\mathrm{d}}{\mathrm{d}\mu} \ln J_i(p_T^J R_J; \mu) = \gamma_J^i(p_T^J R_J; \mu)\,, \tag{3.11}$$

where the jet anomalous dimension is

$$\gamma_J^i(p_T^J R_J; \mu) = 2\Gamma^i_{\mathrm{cusp}}[\alpha_s(\mu)] \ln \frac{\mu}{p_T^J R_J} + \gamma_J^i[\alpha_s(\mu)]\,, \tag{3.12}$$

with the one- and two-loop noncusp anomalous dimensions given by

$$\begin{aligned}
\gamma^q_{J\,0} &= 6C_F\,,\\
\gamma^g_{J\,0} &= 2\beta_0\,,\\
\gamma^q_{J\,1} &= 11.17(5)C_F^2 - 181.30(6)C_F C_A - 7.916(5)C_F n_f T_F\,,\\
\gamma^g_{J\,1} &= 52.898C_A^2 - 215.20C_A C_F - 10.045C_F^2 - 5.1089C_A n_f T_F - 0.37279C_F n_f T_F\,.
\end{aligned} \tag{3.13}$$

The two-loop quark noncusp anomalous dimension $\gamma^q_{J\,1}$ was computed in ref. [61], while we obtain the gluon case $\gamma^g_{J\,1}$ from consistency relations, as discussed in section 3.3.1.

Expanding the jet function J_i according to eq. (3.3), we have

$$\begin{aligned}
J_i^{(0)}(p_T R; \mu) &= 1\,,\\
J_i^{(1)}(p_T R; \mu) &= \Gamma_0^i L_J^2 + \gamma^i_{J\,0} L_J + j_i^{(1)}\,,\\
J_i^{(2)}(p_T R; \mu) &= \frac{\Gamma_0^{i\,2}}{2} L_J^4 + \left(\frac{2\beta_0\Gamma_0^i}{3} + \Gamma_0^i\gamma^i_{J\,0}\right) L_J^3 + \left(\Gamma_1^i + \Gamma_0^i j_i^{(1)} + \beta_0\gamma^i_{J\,0} + \frac{\gamma^{i\,2}_{J\,0}}{2}\right) L_J^2\\
&\quad + \left[(2\beta_0 + \gamma^i_{J\,0}) j_i^{(1)} + \gamma^i_{J\,1}\right] L_J + j_i^{(2)}\,,
\end{aligned} \tag{3.14}$$

where $L_J \equiv \ln[\mu/(p_T^J R_J)]$, and the NLO and NNLO constant terms are given by

$$\begin{aligned}
j_q^{(1)} &= C_F\left(13 - \frac{3\pi^2}{2}\right),\\
j_g^{(1)} &= C_A\left(\frac{5}{6} - \frac{3\pi^2}{2}\right) + \frac{23}{6}\beta_0,\\
j_q^{(2)} &= 4 \times [-1.78(2)C_F^2 - 106.87(2)C_A C_F + 14.072(2)C_F n_f T_F],\\
j_g^{(2)} &\propto \theta_2\,.
\end{aligned} \tag{3.15}$$

The NLO anti-k_T jet functions were calculated in ref. [53], while the NNLO quark jet function has been computed in ref. [61]. The NNLO gluon jet function remains unknown, and its constant term $j^{(2)}$ is therefore treated as a theory nuisance parameter θ_2 and included as part of our perturbative uncertainty, as discussed in section 3.4.

3.1.3 Beam function

The beam function virtuality and rapidity RGEs are given by

$$\begin{aligned}
\mu \frac{\mathrm{d}}{\mathrm{d}\mu} \ln B_i\Big(p_T^{\mathrm{cut}}, x, R_{\mathrm{cut}}; \mu, \frac{\nu}{\omega}\Big) &= \gamma_B^i\Big(\mu, \frac{\nu}{\omega}\Big)\,,\\
\nu \frac{\mathrm{d}}{\mathrm{d}\nu} \ln B_i\Big(p_T^{\mathrm{cut}}, x, R_{\mathrm{cut}}; \mu, \frac{\nu}{\omega}\Big) &= \gamma^i_{\nu,B}(p_T^{\mathrm{cut}}, R_{\mathrm{cut}}; \mu)\,,
\end{aligned} \tag{3.16}$$

JHEP03(2025)155

where the anomalous dimensions are

$$\gamma_B^i\Big(\mu,\frac{\nu}{\omega}\Big) = 2\Gamma^i_{\rm cusp}[\alpha_s(\mu)]\,\ln\frac{\nu}{\omega} + \gamma_B^i[\alpha_s(\mu)]\,,$$
$$\gamma^i_{\nu,B}(p_T^{\rm cut},R_{\rm cut};\mu) = 2\eta^i_\Gamma(p_T^{\rm cut};\mu) + \gamma^i_{\nu,B}[\alpha_s(p_T^{\rm cut}),R_{\rm cut}]\,, \tag{3.17}$$

with

$$\begin{aligned}
\gamma^g_{B\,0} &= 2\beta_0\,, \\
\gamma^g_{B\,1} &= 2\beta_1 + 8C_A\bigg[\Big(-\frac{5}{4}+2(1+\pi^2)\ln 2-6\zeta_3\Big)C_A + \Big(\frac{5}{24}-\frac{\pi^2}{3}+\frac{10}{3}\ln 2\Big)\beta_0\bigg]\,, \\
\gamma^q_{B\,0} &= 6C_F\,, \\
\gamma^q_{B\,1} &= C_F\bigg[(3-4\pi^2+48\zeta_3)C_F + (-14+16(1+\pi^2)\ln 2-96\zeta_3)C_A \\
&\qquad + \Big(\frac{19}{3}-\frac{4\pi^2}{3}+\frac{80}{3}\ln 2\Big)\beta_0\bigg]\,, \\
\gamma^i_{\nu,B\,0}(R_{\rm cut}) &= 0\,, \\
\gamma^i_{\nu,B\,1}(R_{\rm cut}) &= 8C_i\bigg[\Big(\frac{17}{9}-(1+\pi^2)\ln 2+\zeta_3\Big)C_A + \Big(\frac{4}{9}+\frac{\pi^2}{12}-\frac{5}{3}\ln 2\Big)\beta_0\bigg] - \frac{1}{2}C_iC_2(R_{\rm cut})\,,
\end{aligned} \tag{3.18}$$

where $C_i = C_A$ for $i = g$, $C_i = C_F$ for $i = q$, and the $R_{\rm cut}$ dependent part of the rapidity anomalous dimension is given by [16, 62]

$$\begin{aligned}
C_2(R_{\rm cut}) = {}& 2\ln R_{\rm cut}^2\bigg[\Big(1-\frac{8\pi^2}{3}\Big)C_A + \Big(\frac{23}{3}-8\ln 2\Big)\beta_0\bigg] + 15.62C_A - 9.17\beta_0 \\
& + 54.21R_{\rm cut}^2 - 4.40R_{\rm cut}^4 + 0.11R_{\rm cut}^6 + \mathcal{O}(R_{\rm cut}^8)\,,
\end{aligned} \tag{3.19}$$

where the terms without an explicit colour factor assume $n_f = 5$.

As discussed in section 2.3, placing a jet veto can mix the constraints imposed by the measurement on the soft and $n_{a,b}$-collinear sectors leading to the presence of soft-collinear mixing terms at $\mathcal{O}(R_{\rm cut}^2)$ [14]. Various ways for treating these subleading terms have been proposed in the literature. Since we will use the results of ref. [63] for the 2-loop beam functions, we follow their prescription and exponentiate these terms rather than treating them as an additional additive contribution. The rapidity anomalous dimension $\gamma_{\nu,B\,1}$ then takes the form shown above.

The beam function can be written as a convolution between perturbative matching kernels $\mathcal{I}_{ij}(p_T^{\rm cut},R_{\rm cut},\omega,z;\mu,\nu)$ and the standard PDFs $f_j(x,\mu)$,

$$B_i\Big(p_T^{\rm cut},x,R_{\rm cut};\mu,\frac{\nu}{\omega}\Big) = \sum_j\int_x^1\frac{{\rm d}z}{z}\mathcal{I}_{ij}\Big(p_T^{\rm cut},z,R_{\rm cut};\mu,\frac{\nu}{\omega}\Big)\,f_j\Big(\frac{x}{z},\mu\Big). \tag{3.20}$$

The matching kernels can be perturbatively expanded as

$$\mathcal{I}_{ij} = \delta_{ij}\delta(1-z) + \frac{\alpha_s(\mu)}{4\pi}\mathcal{I}_{ij}^{(1)} + \Big(\frac{\alpha_s(\mu)}{4\pi}\Big)^2\mathcal{I}_{ij}^{(2)} + \mathcal{O}(\alpha_s^3)\,. \tag{3.21}$$

Suppressing most arguments for brevity and using

$$L_B^\mu = \ln\frac{\mu}{p_T^{\rm cut}}\,,\quad L_B^\nu = \ln\frac{\nu}{Q}\,, \tag{3.22}$$

JHEP03(2025)155

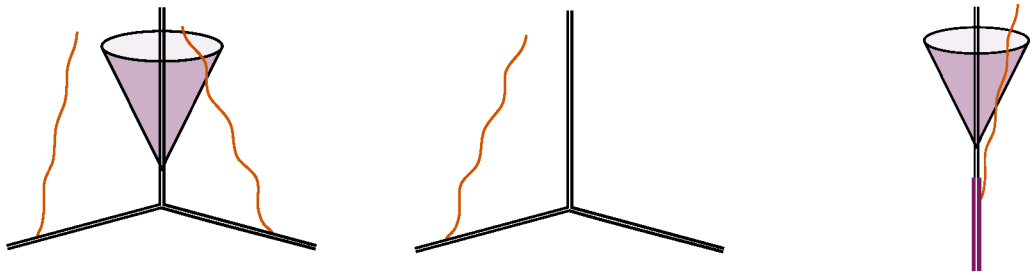

(a) Total-soft S^T (b) Global-soft S_κ (c) Soft-collinear $\mathcal{S}^R$

Figure 1. Depiction of the total soft function S^T (a) present in the $R_J \sim 1$ limit, and of its refactorization into the global soft function S_κ (b) and soft-collinear function $\mathcal{S}^R$ (c) in the $R_J \ll 1$ limit, the latter two appearing in eq. (2.12).

the one- and two-loop matching kernels are given by

$$\begin{aligned}
\mathcal{I}_{ij}^{(1)}(z) &= \delta_{ij}\delta(1-z)\, L_B^\mu(2\Gamma_0^i L_B^\nu + \gamma_{B\,0}^i) - 2L_B^\mu P_{ij}^{(0)}(z) + I_{ij}^{(1)}(z)\,, \\
\mathcal{I}_{ij}^{(2)}(z) &= \delta_{ij}\delta(1-z)\Big\{(L_B^\mu)^2\Big[2(\Gamma_0^i)^2(L_B^\nu)^2 + L_B^\nu(2\beta_0\Gamma_0^i + 2\Gamma_0^i\gamma_{B\,0}^i) + \beta_0\gamma_{B\,0}^i + \frac{(\gamma_{B\,0}^i)^2}{2}\Big] \\
&\qquad + L_B^\mu\Big[2\Gamma_1^i L_B^\nu + \gamma_{B\,1}^i\Big] - \frac{1}{2}\gamma_{\nu\,1}^i(R_{\rm cut})L_B^\nu\Big\} \\
&\quad + P_{ij}^{(0)}(z)\,(L_B^\mu)^2\Big[-4\Gamma_0^i L_B^\nu - 2\beta_0 - 2\gamma_{B\,0}^i\Big] + I_{ij}^{(1)}(z)\, L_B^\mu\Big[2\Gamma_0^i L_B^\nu + 2\beta_0 + \gamma_{B\,0}^i\Big] \\
&\quad - 2L_B^\mu \sum_k I_{ik}^{(1)}(z) \otimes_z P_{kj}^{(0)}(z) - 2L_B^\mu P_{ij}^{(1)}(z) + 2(L_B^\mu)^2 \sum_k P_{ik}^{(0)}(z) \otimes_z P_{kj}^{(0)}(z) \\
&\quad + I_{ij}^{(2)}(R_{\rm cut}, z)\,,
\end{aligned} \tag{3.23}$$

The splitting functions and respective convolutions can e.g. be found in ref. [30]. The finite parts are given by [13, 16, 17]

$$\begin{aligned}
I_{qq}^{(1)}(z) &= 2C_F z\,, \\
I_{gg}^{(1)}(z) &= 0\,, \\
I_{qq}^{(1)}(z) &= 2C_F(1-z)\,, \\
I_{qg}^{(1)}(z) &= 4T_F z(1-z)\,.
\end{aligned} \tag{3.24}$$

At NNLO, the quark and gluon beam functions were computed via a numerical approach in ref. [64, 65]; semi-analytic expressions for both quark and gluon cases later appeared in ref. [62]. We have implemented these expressions up to $\mathcal{O}(R_{\rm cut}^4)$ in SCETlib. The effect of higher order terms $\mathcal{O}(R_{\rm cut}^6)$ is negligible for phenomenologial applications [33].

3.1.4 Soft and soft-collinear functions

In this section we discuss the global soft (S_κ) and soft-collinear ($\mathcal{S}^R$) functions appearing in the factorized cross section in eq. (2.12). To understand their origin, we start by discussing the soft sector in its entirety before taking the $R_J \ll 1$ limit. The total soft function, denoted S^T, is given by the squared matrix element of a set of Wilson lines which can act as sources

JHEP03(2025)155

of soft(-collinear) gluons, where the gauge field has the appropriate soft or soft-collinear momentum scaling. Its definition is given by

$$S_\kappa^T = \frac{1}{N_\kappa} \sum_{X_s} \langle 0|\bar{\mathbf{T}}[Y^\dagger(\{n_i\},\kappa)]|X_s\rangle\langle X_s|\mathbf{T}[Y(\{n_i\},\kappa)]|0\rangle\, \mathcal{M}_{\text{full}}(X_s)\,, \tag{3.25}$$

where $Y(\{n_i\},\kappa)$ collects the set of three soft Wilson lines, one for each external parton. The normalization factor N_κ is chosen such that the tree-level soft function is the identity matrix in colour space. The individual soft Wilson lines are defined as

$$Y_{n_i}^i(x) = \mathbf{P}\exp\left\{ig_s\int_{-\infty}^0 \mathrm{d}s\, n_i\cdot A_s^i(x+sn_i)\right\}, \tag{3.26}$$

for a given incoming parton along the n_i direction, and the representation of the gauge field A_s^i depends on whether the associated particle i is a (anti-)quark or gluon. This total soft function corresponds to the soft function of ref. [37]. For S^T, depicted in figure 1(a), radiation clusters outside the jet are required to have transverse momentum $k_T < p_T^{\text{cut}}$, while radiation inside the jet is unconstrained.

An explicit NLO computation of S^T is presented in appendix B, where we see that it depends on two scales: p_T^{cut} and $p_T^{\text{cut}}R_J$. In the $R_J \sim 1$ limit, these scales are parametrically of the same size and $\ln[\mu/p_T^{\text{cut}}]$ and $\ln[\mu/(p_T^{\text{cut}}R_J)]$ can be simultaneously minimized by choosing $\mu \sim p_T^{\text{cut}}$. However, the factorization of the jet-collinear sector requires us to employ the narrow jet limit $R_J \ll 1$. This makes the two scales parametrically different and therefore requires the factorization of the total soft function into global-soft and soft-collinear functions,

$$S_\kappa^T(p_T^{\text{cut}}, R_{\text{cut}}, R_J, y_J; \mu, \nu) = S_\kappa(p_T^{\text{cut}}, R_{\text{cut}}, y_J; \mu, \nu)\mathcal{S}_j^R(p_T^{\text{cut}}R_J; \mu) + \mathcal{O}(R_J^2)\,, \tag{3.27}$$

each only depending on a single scale p_T^{cut} or $p_T^{\text{cut}}R_J$.

The global-soft function S describes wide-angle radiation and does not probe the (narrow) jet boundary, so it simply requires all clusters to have transverse momentum below p_T^{cut}, as depicted in figure 1(b). Its definition in terms of Wilson lines is therefore similar to that of the total soft function, only with a different measurement function

$$S_\kappa = \sum_{X_s} \langle 0|\bar{\mathbf{T}}[Y^\dagger(\{n_i\},\kappa)]|X_s\rangle\langle X_s|\mathbf{T}[Y(\{n_i\},\kappa)]|0\rangle\, \mathcal{M}_s(X_s)\,, \tag{3.28}$$

where $\mathcal{M}_s$ is now the global measurement, see eq. (2.26), and is independent of R_J. Its virtuality and rapidity RGEs are given by

$$\begin{aligned}
\mu\frac{\mathrm{d}}{\mathrm{d}\mu}\ln S_\kappa(p_T^{\text{cut}}, R_{\text{cut}}, y_J; \mu, \nu) &= \gamma_S^\kappa(p_T^{\text{cut}}, y_J; \mu, \nu)\,,\\
\nu\frac{\mathrm{d}}{\mathrm{d}\nu}\ln S_\kappa(p_T^{\text{cut}}, R_{\text{cut}}, y_J; \mu, \nu) &= \gamma_{\nu,S}^\kappa(p_T^{\text{cut}}, R_{\text{cut}}; \mu)\,.
\end{aligned} \tag{3.29}$$

The anomalous dimensions are

$$\begin{aligned}
\gamma_S^\kappa(p_T^{\text{cut}}, y_J; \mu, \nu) = {}& 2\Gamma_{\text{cusp}}^a[\alpha_s(\mu)]\ln\left(\frac{\mu}{\nu e^{-y_J}}\right) + 2\Gamma_{\text{cusp}}^b[\alpha_s(\mu)]\ln\left(\frac{\mu}{\nu e^{y_J}}\right)\\
&+ 2\Gamma_{\text{cusp}}^j[\alpha_s(\mu)]L_S^\mu + \gamma_S^\kappa[\alpha_s(\mu)]
\end{aligned}$$

JHEP03(2025)155

$$
\begin{aligned}
&= 2(\Gamma^a_{\rm cusp}[\alpha_s(\mu)] + \Gamma^b_{\rm cusp}[\alpha_s(\mu)] + \Gamma^j_{\rm cusp}[\alpha_s(\mu)])L^\mu_S \\
&\quad + 2\Gamma^a_{\rm cusp}[\alpha_s(\mu)]L^a_S + 2\Gamma^b_{\rm cusp}[\alpha_s(\mu)]L^b_S + \gamma^\kappa_S[\alpha_s(\mu)]\,, \\
\gamma^\kappa_{\nu,S}(p_T^{\rm cut}, R_{\rm cut};\mu) &= -\gamma^a_{\nu,B}(p_T^{\rm cut}, R_{\rm cut},\mu) - \gamma^b_{\nu,B}(p_T^{\rm cut}, R_{\rm cut},\mu)\,,
\end{aligned}
\tag{3.30}
$$

where the beam rapidity anomalous dimensions $\gamma_{\nu,B}$ are given in eqs. (3.17) and (3.18), and we use the shorthand

$$
L^\mu_S = \ln\frac{\mu}{p_T^{\rm cut}}\,, \qquad L^a_S = \ln\Big(\frac{e^{y_J}p_T^{\rm cut}}{\nu}\Big)\,, \qquad L^b_S = \ln\Big(\frac{e^{-y_J}p_T^{\rm cut}}{\nu}\Big)\,. \tag{3.31}
$$

RG consistency only fixes the sum of the anomalous dimension of the global soft function and the soft-collinear function. The individual terms are not known at two-loop order, and we therefore account for the splitting of the total soft anomalous dimension into the two pieces using a theory nuisance parameter, as discussed in section 3.4. The logarithmic terms of the global soft function at a given order are fixed by its RGE and lower-order constant terms. For definiteness, we still show how it can be directly calculated at NLO:

$$
S_{\kappa,\rm bare}(p_T^{\rm cut}, R_{\rm cut}, y_J) = 1 - \frac{\alpha_s}{\pi^{2-\epsilon}}(e^{\gamma_E}\mu^2)^\epsilon \sum_{l<m} \mathbf{T}_l\cdot\mathbf{T}_m \int {\rm d}^d k\,\delta(k^2)\frac{n_l\cdot n_m}{(n_l\cdot k)(n_m\cdot k)}\,\Theta(p_T^{\rm cut} - k_T),
\tag{3.32}
$$

with $l, m \in \{a, b, j\}$. Following the same procedure taken in the calculation of the total soft function (appendix B) this yields

$$
S^{(1)}_\kappa(p_T^{\rm cut}, y_J;\mu,\nu) = (C_a + C_b + C_j)\Gamma_0\big(L^\mu_S\big)^2 + 2\Gamma_0\big[C_a L^a_S + C_b L^b_S\big]L^\mu_S + s^{(1)}_\kappa\,. \tag{3.33}
$$

At NLO the constant term is

$$
s^{(1)}_\kappa = -(C_a + C_b + C_j)\frac{\pi^2}{6}\,. \tag{3.34}
$$

The NNLO soft function is

$$
\begin{aligned}
S^{(2)}_\kappa(p_T^{\rm cut}, R_{\rm cut}, y_J;\mu,\nu) &= \frac{1}{2}(C_a + C_b + C_j)^2\Gamma_0^2\big(L^\mu_S\big)^4 \\
&\quad + \frac{2}{3}(C_a + C_b + C_j)\Gamma_0\Big[\beta_0 + 3\Gamma_0\big(C_a L^a_S + C_b L^b_S\big)\Big]\big(L^\mu_S\big)^3 \\
&\quad + \Big\{(C_a + C_b + C_j)(\Gamma_0 s^{(1)}_\kappa + \Gamma_1) + 2\Gamma_0\big[C_a L^a_S + C_b L^b_S\big] \\
&\qquad \times \Big[\beta_0 + \Gamma_0\big(C_a L^a_S + C_b L^b_S\big)\Big]\Big\}\big(L^\mu_S\big)^2 \\
&\quad + \Big\{2s^{(1)}_\kappa\beta_0 + \gamma^\kappa_{S\,1} + 2\big[s^{(1)}_\kappa\Gamma_0 + \Gamma_1\big]\big[C_a L^a_S + C_b L^b_S\big]\Big\}L^\mu_S \\
&\quad + \gamma^\kappa_{\nu,S\,1}\ln\frac{\nu}{p_T^{\rm cut}} + s^{(2)}_\kappa\,,
\end{aligned}
\tag{3.35}
$$

where we have used $\gamma^\kappa_{S\,0} = \gamma^\kappa_{\nu,S\,0} = 0$ to simplify the expression. The two-loop constant term $s^{(2)}_\kappa$ is unknown and will be parametrized in terms of a theory nuisance parameter, as explained in section 3.4. Note that the dependence of the global soft function on $R_{\rm cut}$ starts at two-loop order and enters through the rapidity anomalous dimension and the two-loop

JHEP03(2025)155

constant term. In principle, the presence of logarithms of e^{-y_J} in eqs. (3.33) and (3.35) implies that a further factorization is possible. However, here we always consider the case where the jet is well separated from the beams, $n_a \cdot n_J \sim n_b \cdot n_J \sim \mathcal{O}(1)$, such that the rapidity dependence can be treated in fixed-order perturbation theory. Moreover, these logarithms vanish for the most phenomenologically relevant channel, $gg \to Hg$.

We now turn to the soft-collinear function $\mathcal{S}^R$, which is depicted in figure 1(c). As explained in section 2.3, the soft-collinear function arises as a correction to the global soft function. The latter applies the p_T-veto to soft radiation everywhere, including inside the jet region. However, radiation inside the jet should not be subject to a veto. The collinear nature of soft-collinear radiation allows it to resolve the jet boundary and correct for this. Its RGE is given by

$$\mu \frac{\mathrm{d}}{\mathrm{d}\mu} \ln \mathcal{S}_i^R(p_T^{\mathrm{cut}} R_J; \mu) = \gamma_{\mathcal{S}}^i(p_T^{\mathrm{cut}} R_J; \mu) \tag{3.36}$$

where the anomalous dimension is

$$\gamma_{\mathcal{S}}^i(p_T^{\mathrm{cut}} R_J; \mu) = -2\Gamma_{\mathrm{cusp}}^i[\alpha_s(\mu)] \ln\Big(\frac{\mu}{p_T^{\mathrm{cut}} R_J}\Big) + \gamma_{\mathcal{S}}^i[\alpha_s(\mu)]\,, \tag{3.37}$$

with

$$\gamma_{\mathcal{S}\,0}^i = 0\,. \tag{3.38}$$

$\gamma_{\mathcal{S}\,1}^i$ depends on the unknown split of the total soft anomalous dimension into global and soft-collinear pieces, which is parameterized by a nuisance parameter.

The definition of the soft-collinear function is

$$\mathcal{S}_i^R(p_T^{\mathrm{cut}} R_J) = \frac{1}{d_i(N_c)} \sum_{X_{sc}} \mathrm{Tr}[\langle 0|\bar{T}[V_{n_J}^\dagger X_{n_J}]|X_{sc}\rangle\langle X_{sc}|T[X_{n_J}^\dagger V_{n_J}]|0\rangle] \mathcal{M}_{sc}(X_{sc})\,, \tag{3.39}$$

where the representation of the Wilson lines depends on the flavour of the parton initiating the jet and $d_j(N_c)$ denotes the dimension of this representation, i.e. $d_q = N_c$ and $d_g = N_c^2 - 1$. $X_n^\dagger$ and $V_n^\dagger$ are soft-collinear Wilson lines defined as

$$\begin{aligned} X_n^\dagger(x) &= \mathbf{P}\Big\{ \exp\Big[-\mathrm{i}g \int_0^\infty \mathrm{d}s\, n \cdot A_{sc}(x + sn)\Big]\Big\}\,, \\ V_n^\dagger(x) &= \mathbf{P}\Big\{ \exp\Big[-\mathrm{i}g \int_0^\infty \mathrm{d}s\, \bar{n} \cdot A_{sc}(x + s\bar{n})\Big]\Big\}\,, \end{aligned} \tag{3.40}$$

where A_{sc} is the soft-collinear gluon field. The subscript n does not refer to the direction of the Wilson line, but indicates that these soft-collinear gluons are collinear to the n direction.

At NLO, where there is only a single real emission with momentum k_{sc}, the soft-collinear function is given by

$$\mathcal{S}_{i,\mathrm{bare}}^R(p_T^{\mathrm{cut}} R_J) = 1 - \frac{\alpha_s}{\pi^{2-\epsilon}} (e^{\gamma_E}\mu^2)^\epsilon\, C_i \int \mathrm{d}^d k\, \delta(k^2)\, \frac{n_J \cdot \bar{n}_J}{(n_J \cdot k)(\bar{n}_J \cdot k)}\, \mathcal{M}_{sc}(X_{sc})\,, \tag{3.41}$$

where the one-loop measurement function is (see eq. (2.20))

$$\begin{aligned} \mathcal{M}_{sc}^{(1)}(k_{sc}) &= \Theta(k_T^{sc} - p_T^{\mathrm{cut}})\Theta(R_J - \Delta R^{sc}) \\ &= \Big[1 - \Theta(p_T^{\mathrm{cut}} - k_T^{sc})\Big]\,\Theta(R_J - \Delta R^{sc})\,, \end{aligned} \tag{3.42}$$

JHEP03(2025)155

and the light-like vectors n_J and $\bar{n}_J$ are defined in eq. (2.10). This yields the NLO expression

$$\mathcal{S}_j^{R,(1)}(p_T^{\rm cut} R_J;\mu) = -\Gamma_0^i L_R^2 + \gamma_{\mathcal{S}\,0}^i L_R + s_i^{R,(1)}\,, \tag{3.43}$$

where $L_R = \ln(\mu/(p_T^{\rm cut} R_J))$ and the NLO constant piece is

$$s_i^{R,(1)} = C_i\,\frac{\pi^2}{6}\,. \tag{3.44}$$

At NNLO we have

$$\begin{aligned}\mathcal{S}_j^{R,(2)}(p_T^{\rm cut} R_J;\mu) = \frac{\Gamma_0^{j\,2}}{2} L_R^4 - \Gamma_0^j\Big(\frac{2}{3}\beta_0 + \gamma_{\mathcal{S}\,0}^j\Big) L_R^3 + \Big[\beta_0\gamma_{\mathcal{S}\,0}^j + \frac{\gamma_{\mathcal{S}\,0}^{j\,2}}{2} - \Gamma_0^j s_j^{R,(1)} - \Gamma_1^j\Big] L_R^2 \\ + \Big[(2\beta_0 + \gamma_{\mathcal{S}\,0}^j) s_j^{R,(1)} + \gamma_{\mathcal{S}\,1}^j\Big] L_R + s_j^{R,(2)}\,,\end{aligned} \tag{3.45}$$

where the NNLO constant will be treated as a theory nuisance parameter, as described in section 3.4.

3.1.5 Nonglobal logarithms

As explained in section 2, the function $S_{\rm NG}(p_T^{\rm cut}/p_T^J)$ encodes the nonglobal logarithms arising from correlated emissions inside and outside the signal jet. After a boost in the jet direction (exploiting type-III reparametrization invariance), the inside and outside of the jet can be turned into complementary hemispheres, implying that the leading NGLs are given by the same universal function as for the hemisphere masses. We will work in the large N_c approximation (the leading NGLs without this approximation have been studied in ref. [66]). Rather than using the fit of ref. [67], we employ the solution to the BMS equation [68] up to five-loop order [69],

$$\mathcal{S}_q^{\rm NG}\Big(\frac{p_T^{\rm cut}}{p_T^J}\Big) = 1 - \frac{\pi^2}{24}\widehat{L}^2 + \frac{\zeta_3}{12}\widehat{L}^3 + \frac{\pi^4}{34560}\widehat{L}^4 + \Big(-\frac{\pi^2\zeta_3}{360} + \frac{17\zeta_5}{480}\Big)\widehat{L}^5 + \mathcal{O}(L^6)\,, \tag{3.46}$$

where

$$\widehat{L} = \frac{\alpha_s N_c}{\pi}\ln\frac{p_T^J}{p_T^{\rm cut}}\,. \tag{3.47}$$

The convergence of this expression for the kinematic region we are interested in can be seen in figure 2. For the indicative values, $p_T^J = 120\,\text{GeV}$, $p_T^{\rm cut} = 30\,\text{GeV}$, $R_J = 0.4$, we have $\alpha_s(\mu = p_T^{\rm cut} R_J) = 0.171$ and $\widehat{L} = 0.226$, and the expansion reads

$$\mathcal{S}_q^{\rm NG} = 1 - 2.10\times10^{-2} + 1.15\times10^{-3} + 7.34\times10^{-6} + 2.22\times10^{-6} + \cdots\,. \tag{3.48}$$

Given the excellent convergence beyond three-loop order, we employ the five-loop result in eq. (3.46) as a proxy for the resummed tower of leading NGLs. We therefore want to keep all terms in eq. (3.46) in the resummation region, while in the fixed-order region the nonglobal logs should be expanded in α_s to the same order as the rest of the cross section. A simple way to achieve this is by defining

$$\mathcal{S}_i^{\rm NG}(p_T^{\rm cut}, p_T^J;\mu_{\mathcal{S}},\mu_J) = \mathcal{S}_{i\,\rm resum}^{\rm NG}\Big(\frac{\mu_{\mathcal{S}}}{\mu_J}\Big)\,\mathcal{S}_{i\,\rm FO}^{\rm NG}\Big(\frac{p_T^{\rm cut}}{\mu_{\mathcal{S}}}\frac{\mu_J}{p_T^J}\Big)\,, \tag{3.49}$$

JHEP03(2025)155

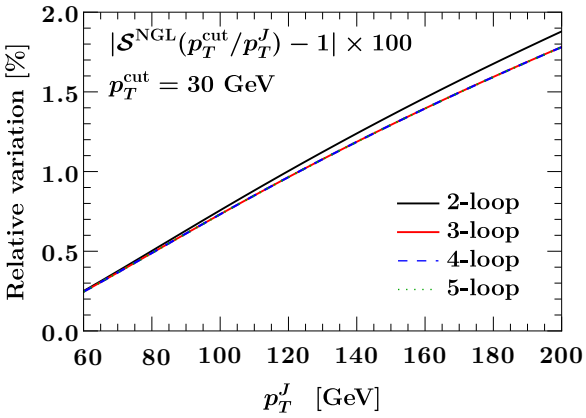

Figure 2. The relative correction from nonglobal logarithms up to 2-loop, 3-loop, 4-loop and 5-loop order, using $\alpha_s(M_Z) = 0.118$ as a representative value. For the region of interest the 2-loop thus affects the cross section at the percent level, the 3-loop at the permille level, and beyond it is negligible.

where both $\mathcal{S}_{i\,\rm resum}^{\rm NG}$ and $\mathcal{S}_{i\,\rm FO}^{\rm NG}$ are obtained from eq. (3.46), with the former treated as an evolution kernel (and the full five-loop expansion used), while the latter is considered as a boundary condition and is therefore expanded to order α_s^2. The scales $\mu_{\mathcal{S}}$ and μ_J take different values in the resummation and fixed-order regions: in the resummation region, they are chosen to minimize the size of large logarithms as $\mu_{\mathcal{S}} = p_T^{\rm cut} R_J$ and $\mu_J = p_T^J R_J$, while in the fixed-order region they take the common value $\mu_{\mathcal{S}} = \mu_J = \mu_{\rm FO}$. This ensures that eq. (3.49) behaves appropriately in the two limits, since in each we have:

$$\begin{aligned}
&\text{Resummation region:} \quad \mathcal{S}_i^{\rm NG}(p_T^{\rm cut}, p_T^J; \mu_{\mathcal{S}} = p_T^{\rm cut} R_J, \mu_J = p_T^J R_J) = \mathcal{S}_{i\,\rm resum}^{\rm NG}\left(\frac{p_T^{\rm cut}}{p_T^J}\right), \\
&\text{Fixed order region:} \quad \mathcal{S}_i^{\rm NG}(p_T^{\rm cut}, p_T^J; \mu_{\mathcal{S}} = \mu_{\rm FO}, \mu_J = \mu_{\rm FO}) = \mathcal{S}_{i\,\rm FO}^{\rm NG}\left(\frac{p_T^{\rm cut}}{p_T^J}\right).
\end{aligned} \tag{3.50}$$

We will thus use eq. (3.49) in our numerical implementation.

3.2 Validation of the singular structure

To check whether the factorization formula in eq. (2.12) reproduces all the leading-power logarithms of the fixed-order result, we examine the behaviour of the nonsingular cross section differential in $\ln p_T^{\rm 2nd}$ in the limit $p_T^{\rm 2nd} \to 0$. (We use $p_T^{\rm cut}$ for the integrated cross section and $p_T^{\rm 2nd}$ for the corresponding differential cross section.) The nonsingular cross section is defined as

$$\frac{{\rm d}\sigma^{\rm ns}}{{\rm d}\ln p_T^{\rm 2nd}} \equiv \frac{{\rm d}\sigma^{\rm FO}}{{\rm d}\ln p_T^{\rm 2nd}} - \frac{{\rm d}\sigma^{\rm sing}}{{\rm d}\ln p_T^{\rm 2nd}}, \tag{3.51}$$

where ${\rm d}\sigma^{\rm FO}/{\rm d}\ln p_T^{\rm 2nd}$ is the full fixed-order cross section and ${\rm d}\sigma^{\rm sing}/{\rm d}\ln p_T^{\rm 2nd}$ is given by the factorization formula in eq. (2.12) made differential, which reproduces the singular terms in

JHEP03(2025)155

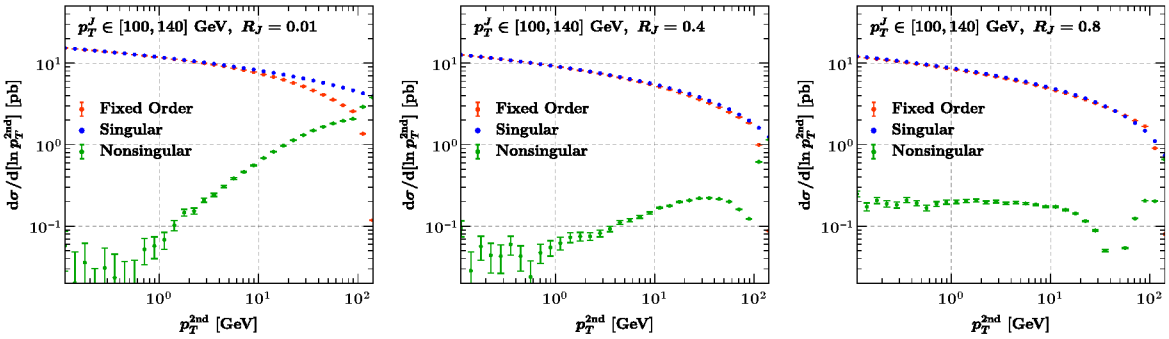

Figure 3. Full fixed order (red), singular (blue) and nonsingular (green) at NLO, differential in $\ln p_T^{2\text{nd}}$, for $R_J = 0.01, 0.4$ and 0.8. Wee see that the small $p_T^{2\text{nd}}$ behaviour of the nonsingular is linear for $R_J = 0.01$ and constant for large R_J, which implies the presence of $R_J^2 \ln p_T^{\text{cut}}$ power corrections.

$p_T^{2\text{nd}}$ of the fixed-order result. At order α_s these leading-power singular terms take the form

$$\frac{\mathrm{d}\sigma^{\text{FO}}}{\mathrm{d}p_T^{2\text{nd}}} = \alpha_s\bigg(c_{-1}\,\delta(p_T^{2\text{nd}}) + c_0\frac{1}{[p_T^{2\text{nd}}]_+} + c_1\bigg[\frac{\ln p_T^{2\text{nd}}}{p_T^{2\text{nd}}}\bigg]_+ + \text{p.c.}\bigg)$$
$$\Longrightarrow \quad \frac{\mathrm{d}\sigma^{\text{FO}}}{\mathrm{d}\ln p_T^{2\text{nd}}} = \alpha_s(c_0 + c_1 \ln p_T^{2\text{nd}} + \text{p.c.}), \tag{3.52}$$

where c_{-1}, c_0 and c_1 are constants that do not depend on $p_T^{2\text{nd}}$ and p.c. denotes power corrections. If the singular piece correctly captures the c_0 and c_1 terms above, these will not be present in the nonsingular difference, and we therefore expect $\mathrm{d}\sigma^{\text{ns}}/\mathrm{d}\ln p_T^{2\text{nd}} \to 0$ as $p_T^{2\text{nd}} \to 0$.

In figure 3, we show the nonsingular, singular and full fixed-order results for various values of the jet radius R_J, where the fixed NLO calculation for Higgs+jet used to obtain the nonsingular is provided by the Monte Carlo event generator GENEVA [70]. We observe that for very small values of the jet radius (e.g. $R_J = 0.01$) the nonsingular cross section goes to zero as $p_T^{\text{cut}} \to 0$, as expected. In fact, its linear behaviour at small $p_T^{2\text{nd}}$ in the log-log plot is consistent with the presence of a $p_T^{\text{cut}} \ln p_T^{\text{cut}}$ power correction in $\sigma(p_T^{\text{cut}})$. For larger values of the jet radius (e.g. $R_J = 0.8$), however, we see that the nonsingular tends to a constant in the small $p_T^{2\text{nd}}$ limit, implying that the singular cross section is insufficient to fully reproduce the c_0 term in eq. (3.52) for larger values of R_J. The worsening of the behaviour for increasing R_J is due to the presence of terms of $\mathcal{O}(R_J^2)$ and $\mathcal{O}(R_J^2 \ln p_T^{\text{cut}})$ in the nonsingular cross section $\sigma(p_T^{\text{cut}})$. Since our factorization formula assumes $R_J \ll 1$, these terms are formally a power correction, which cannot be expected to be reproduced by the singular. However, figure 3 shows that they can be numerically sizeable even for intermediate values of $R_J = 0.4$, since they are only suppresed by R_J^2 but are effectively singular in p_T^{cut}, and we would therefore like to include them explicitly.

The factorization of the soft sector into the global soft $S_\kappa(p_T^{\text{cut}}; \mu, \nu)$ and the soft-collinear $\mathcal{S}^R(p_T^{\text{cut}} R_J; \mu)$ functions relies on the limit $R_J \ll 1$ and is valid up to $\mathcal{O}(R_J^2)$ terms, which are precisely the R_J^2 power corrections we wish to retain. To compute them we therefore consider the total soft function in eq. (3.27) including R_J^2 corrections. The full calculation

JHEP03(2025)155

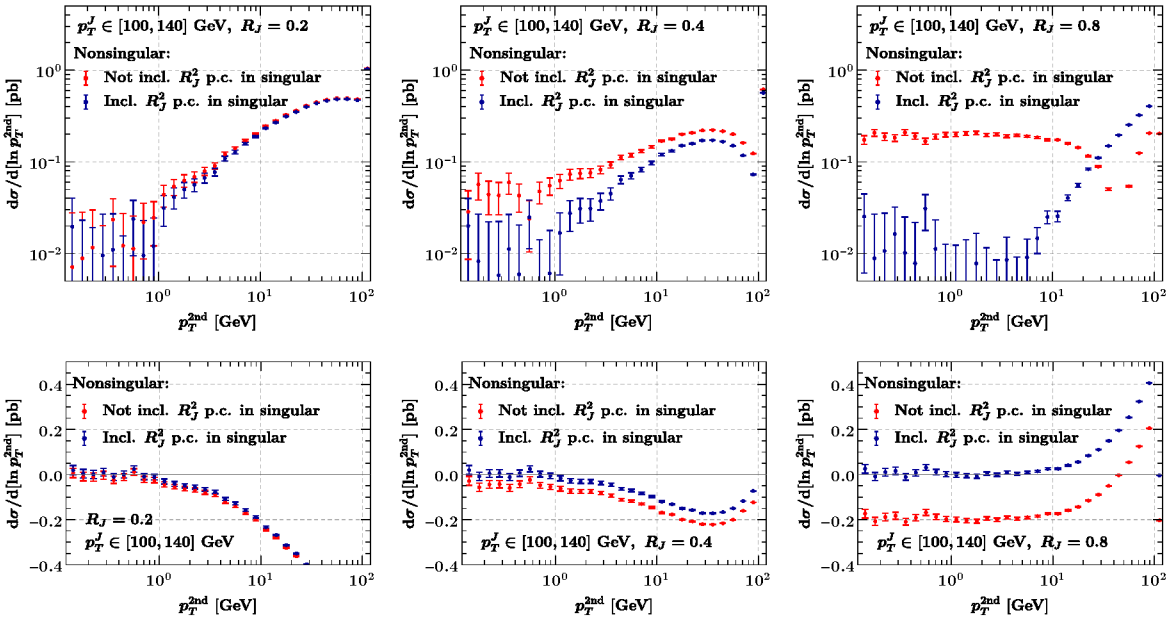

Figure 4. Nonsingular with (blue) and without (red) $R_J^2 \ln p_T^{\mathrm{cut}}$ T power corrections for $R_J = 0.2$ (left), 0.4 (middle) and 0.8 (right), using log-log axes (top) and log-linear axes (bottom).

is laid out in appendix B, and the NLO result is

$$
\begin{aligned}
S_\kappa^{T,(1)}(p_T^{\mathrm{cut}}, R_J, \mu) = (C_a + C_b)\Bigg[&- 4\ln^2\Big(\frac{\mu}{p_T^{\mathrm{cut}}}\Big) - 8\ln\Big(\frac{\mu}{p_T^{\mathrm{cut}}}\Big)\ln\Big(\frac{\nu}{\mu}\Big) - \frac{\pi^2}{6} \\
&+ 2R_J^2 \ln\left(\frac{\mu}{p_T^{\mathrm{cut}} R_J}\right) + R_J^2\Bigg] + 8 y_J (C_a - C_b)\ln\Big(\frac{\mu}{p_T^{\mathrm{cut}}}\Big) \\
&+ C_j\Bigg[4\ln^2\Big(\frac{\mu}{p_T^{\mathrm{cut}}}\Big) - 4\ln^2\Big(\frac{\mu}{p_T^{\mathrm{cut}} R_J}\Big) - R_J^2 \ln\left(\frac{\mu}{p_T^{\mathrm{cut}} R_J}\right) + \frac{R_J^2}{6}\Bigg].
\end{aligned}
\tag{3.53}
$$

Note that besides the R_J^2 power corrections (highlighted in red), the above expression also contains the full analytic dependence in $\ln R_J$, which was missing in ref. [37]. The effects of including the R_J^2 power corrections are displayed in figure 4. As is clear, including the power corrections remove the constant offset at small p_T^{cut} that was visible in figure 3.

Given that the power corrections in the soft sector are accompanied by logarithms of $\mu/(p_T^{\mathrm{cut}} R_J)$, it makes sense to absorb them into the soft-collinear function by making the replacements

$$
\begin{aligned}
\gamma_{\mathcal{S}\,0}^j \to \tilde{\gamma}_{\mathcal{S}\,0}^\kappa &= \gamma_{\mathcal{S}\,0}^j + R_J^2\,(2C_a + 2C_b - C_j)\,, \\
s_j^{R,(1)} \to \tilde{s}_j^{R,(1)} &= s_j^{R,(1)} + \Big(C_a + C_b + \frac{1}{6}C_j\Big)R_J^2\,.
\end{aligned}
\tag{3.54}
$$

The inclusion of R_J^2 power corrections in the soft-collinear anomalous dimension introduces a scale dependence that must be cancelled elsewhere to maintain RGE consistency. Since the only other function that exhibits R_J dependence is the jet function, we also make the replacement

$$
\gamma_{J\,0}^j \to \tilde{\gamma}_{J\,0}^\kappa = \gamma_{J\,0}^j - R_J^2\,(2C_a + 2C_b - C_j)\,. \tag{3.55}
$$

JHEP03(2025)155

Order	Boundary conditions	Anomalous dimensions γ_i (noncusp)	Anomalous dimensions Γ_{cusp}, β	FO matching (nonsingular)
LL	1	-	1-loop	-
NLL	1	1-loop	2-loop	-
NLL′ (+NLO)	α_s	1-loop	2-loop	α_s
NNLL (+NLO)	α_s	2-loop	3-loop	α_s
NNLL′ (+NNLO)	α_s^2	2-loop	3-loop	α_s^2
N^{3}LL (+NNLO)	α_s^2	3-loop	4-loop	α_s^2

Table 2. Definition of resummation orders. The (+N^{n}LO) in the order refers to whether or not the nonsingular $\mathcal{O}(\alpha_s^n)$ corrections in the last column are included.

We stress that although we are able to make these replacements to absorb R_J^2 terms into the leading-power (with respect to R_J) resummation, we do not claim that this necessarily correctly resums the $\ln(p_T^{\text{cut}}/p_T^J)$ logarithms at the subleading $\mathcal{O}(R_J^2)$ at either NLL or NLL′.

3.3 Resummation

The ingredients necessary to obtain a given resummed accuracy are shown in table 2. To reach NNLL′, we require the 3-loop cusp anomalous dimension and the 2-loop noncusp anomalous dimensions and 2-loop boundary conditions for the various functions.

3.3.1 Anomalous dimensions from consistency relations

Some of the perturbative ingredients at $\mathcal{O}(\alpha_s^2)$ that are needed at NNLL′ remain, at present, unknown. Specifically, these are the 2-loop noncusp anomalous dimensions and constant terms of the global soft, soft-collinear and gluon jet function. We can deduce most of the missing anomalous dimensions by demanding RGE consistency, which implies that

$$\gamma_H^\kappa + \gamma_S^\kappa + \gamma_{\mathcal{S}}^j + \gamma_J^j + \gamma_B^a + \gamma_B^b = 0. \tag{3.56}$$

However, no such constraints hold for the unknown 2-loop constant terms. The remaining independent unknowns will be treated as theory nuisance parameters, which we vary in order to estimate the uncertainties due to these missing higher order corrections, as discussed in section 3.4.

We first ignore the factorization of the total soft function into global and soft-collinear parts. The consistency relations must hold separately for cusp and noncusp parts, where the latter are in particular free of any kinematic dependence. Considering the $qg \to Hq$ channel, we have

$$\gamma_{S,T}^{qgq} + \gamma_B^q + \gamma_B^g + \gamma_H^{qgq} + \gamma_J^q = 0\,, \tag{3.57}$$

where the total soft anomalous dimension $\gamma_{S,T}$ is given by

$$\gamma_{S,T}^{qgq} = \gamma_S^{qgq} + \gamma_{\mathcal{S}}^q\,. \tag{3.58}$$

JHEP03(2025)155

The two-loop quark jet anomalous dimension $\gamma^q_{J\,1}$ is known [61], as are the relevant hard and beam anomalous dimensions. Using (3.57), we are then able to deduce $\gamma^{qgq}_{S,T\,1}$.

Together with the fact that $\gamma^{qgq}_{S,T\,1} = \gamma^{q\bar{q}g}_{S,T\,1}$, we can then extract $\gamma^g_{J\,1}$ from the $q\bar{q} \to Hg$ channel

$$\gamma^g_J = -(\gamma^{q\bar{q}g}_{S,T} + 2\gamma^q_B + \gamma^{q\bar{q}g}_H)\,. \tag{3.59}$$

By considering $gg \to Hg$, we can then also obtain the total soft noncusp anomalous dimension for the ggg channel,

$$\gamma^{ggg}_{S,T} = -(2\gamma^g_B + \gamma^{ggg}_H + \gamma^g_J)\,. \tag{3.60}$$

We are thus able to determine all anomalous dimensions at 2-loop order so far. However, considering the further factorization of the total soft function into global soft and soft-collinear functions, we do not have sufficient constraints to determine how the total soft noncusp anomalous dimension is split into the global soft and soft-collinear ones, for which we resort to using a theory nuisance parameter as discussed in section 3.4.

3.3.2 Renormalization group evolution

We minimize the size of the logarithms associated with each of the hard, soft, soft-collinear, beam and jet functions by evaluating them at their canonical scales

$$\begin{aligned}
&\mu_H = \sqrt{(p_T^H)^2 + m_H^2}, \qquad && \mu_J = p_T^J R_J, \qquad && \mu_{\mathcal{S}} = p_T^{\text{cut}} R_J, \qquad && \mu_S = \mu_B = p_T^{\text{cut}},\\
&\nu_S = p_T^{\text{cut}}, && \nu_{B\,a,b} = \omega_{a,b}\,.
\end{aligned} \tag{3.61}$$

We then RG-evolve the individual functions to common μ and ν scales via the following solutions to their RGEs in eqs. (3.8), (3.11), (3.16), (3.29) and (3.36). The solution to the virtuality evolution equations can be written as $F(\mu) = F(\mu_0)\,U_F(\mu_0,\mu)$, where the evolution kernels U_F are given by

$$\begin{aligned}
U_J^j(p_T^J R_J;\mu_0,\mu) &= \exp\Big[2K^j_\Gamma(\mu_0,\mu) + K^j_{\gamma_J}(\mu_0,\mu)\Big]\Big(\frac{\mu_0}{p_T^J R_J}\Big)^{2\eta^j_\Gamma(\mu_0,\mu)}\,,\\
U_{\mathcal{S}^R}^j(p_T^{\text{cut}} R_J;\mu_0,\mu) &= \exp\Big[-2K^j_\Gamma(\mu_0,\mu) + K^j_{\gamma_{\mathcal{S}}}(\mu_0,\mu)\Big]\Big(\frac{\mu_0}{p_T^{\text{cut}} R_J}\Big)^{-2\eta^j_\Gamma(\mu_0,\mu)}\,,\\
U_S^\kappa(p_T^{\text{cut}}, y_J;\nu;\mu_0,\mu) &= \exp\Big[2K^a_\Gamma(\mu_0,\mu) + 2K^b_\Gamma(\mu_0,\mu) + 2K^j_\Gamma(\mu_0,\mu) + K^\kappa_{\gamma_S}(\mu_0,\mu)\Big]\\
&\quad\times\Big(\frac{\mu_0}{\nu e^{-y_J}}\Big)^{2\eta^a_\Gamma(\mu_0,\mu)}\Big(\frac{\mu_0}{\nu e^{y_J}}\Big)^{2\eta^b_\Gamma(\mu_0,\mu)}\Big(\frac{\mu_0}{p_T^{\text{cut}}}\Big)^{2\eta^j_\Gamma(\mu_0,\mu)}\,,\\
U_B^a(\omega;\nu;\mu_0,\mu) &= \exp\Big[K^a_{\gamma_B}(\mu_0,\mu)\Big]\Big(\frac{\nu}{\omega}\Big)^{2\eta^a_\Gamma(\mu_0,\mu)}\,,\\
U_H^\kappa(\{s_{ik}\},\mu_0,\mu) &= \exp\Big[2K^a_\Gamma(\mu_0,\mu) + 2K^b_\Gamma(\mu_0,\mu) + 2K^j_\Gamma(\mu_0,\mu) + K^\kappa_{\gamma_H}(\mu_0,\mu)\Big]\\
&\quad\times\Big(\frac{s_{bJ}\mu_0^2}{s_{ab}s_{aJ}}\Big)^{\eta^a_\Gamma(\mu_0,\mu)}\Big(\frac{s_{aJ}\mu_0^2}{s_{ab}s_{bJ}}\Big)^{\eta^b_\Gamma(\mu_0,\mu)}\Big(\frac{s_{ab}\mu_0^2}{s_{aJ}s_{bJ}}\Big)^{\eta^J_\Gamma(\mu_0,\mu)}\,,
\end{aligned} \tag{3.62}$$

where K^i_Γ, K^i_γ and η^i_Γ are given in appendix C. We remind the reader that we also include the R_J^2 power corrections by making the replacement $\gamma_{\mathcal{S},J} \to \tilde{\gamma}_{\mathcal{S},J}$ in the above formulas, where $\tilde{\gamma}_{\mathcal{S},J}$ are defined in eqs. (3.54) and (3.55).

The rapidity evolution equations yield solutions of the form $F(\nu) = F(\nu_0)V(\nu_0, \nu)$ with the rapidity evolution kernels

$$V_S^\kappa(p_T^{\rm cut}; \mu_0; \nu_0, \nu) = \left(\frac{\nu}{\nu_0}\right)^{-\gamma^a_{\nu,B}(p_T^{\rm cut}, R_{\rm cut}; \mu_0) - \gamma^b_{\nu,B}(p_T^{\rm cut}, R_{\rm cut}; \mu_0)},$$
$$V_B^i(p_T^{\rm cut}; \mu_0; \nu_0, \nu) = \left(\frac{\nu}{\nu_0}\right)^{\gamma^i_{\nu,B}(p_T^{\rm cut}, R_{\rm cut}; \mu_0)}. \tag{3.63}$$

3.3.3 Profile scales

As we transition from the resummation region, where $p_T^{\rm cut} \ll Q$, to the fixed-order region, where $p_T^{\rm cut} \sim Q$, the resummation needs to be turned off. This is accomplished by arranging a transition of the canonical scales in eq. (3.61) to a common fixed-order scale $\mu_{\rm FO}$ using profile scales [71, 72]. Because the fixed-order scales can be varied, we define the central value as

$$\mu^c_{\rm FO} = \sqrt{(p_T^H)^2 + m_H^2}\,, \tag{3.64}$$

such that

$$\mu_{\rm FO} = \mu^c_{\rm FO} 2^{V_{\rm FO}}\,, \tag{3.65}$$

where $V_{\rm FO} \in \{0, 1, -1\}$ and implements the usual factor of two variations (we discuss the full set of scale variations in section 3.4). The scales entering in the resummed cross section then take the form

$$\mu_H = \mu_{\rm FO}\,, \tag{3.66}$$
$$\mu_X = \mu_{\rm FO}\, f_{\rm run}\left(\xi, \frac{\mu_X^{\rm canon}}{\mu^c_{\rm FO}}\right) f_{\rm vary}(\xi)^{V_X}\,, \tag{3.67}$$
$$\nu_Y = \mu_{\rm FO}\, f_{\rm run}\left(\xi, \frac{\nu_Y^{\rm canon}}{\mu^c_{\rm FO}}\right) f_{\rm vary}(\xi)^{W_Y}\,, \tag{3.68}$$

where $X \in \{J, S, \mathcal{S}, B\}$, $Y \in \{S, B\}$, the scales $\mu_X^{\rm canon}, \nu_X^{\rm canon}$ are given in eq. (3.61) and the variation factors $V_X, W_Y \in \{0, 1, -1\}$. The function $f_{\rm vary}$ is used to turn off the resummation scale variations gradually as we enter the fixed-order region of phase space. The argument ξ of the profile functions is a dimensionless function of $p_T^{\rm cut}$ and the hard kinematics which measures how far along the transition a given phase space point lies. The ξ dependence of the profile function $f_{\rm run}(\xi, y)$ factorizes as

$$f_{\rm run}(\xi, y) = g_{\rm run}(\xi)\, y + [1 - g_{\rm run}(\xi)]\,, \tag{3.69}$$

where

$$g_{\rm run}(x) = \begin{cases} 1 & 0 < x \le x_1\,, \\ 1 - \frac{(x-x_1)^2}{(x_2-x_1)(x_3-x_1)} & x_1 < x \le x_2\,, \\ \frac{(x-x_3)^2}{(x_3-x_1)(x_3-x_2)} & x_2 < x \le x_3\,, \\ 0 & x_3 \le x\,, \end{cases} \tag{3.70}$$

JHEP03(2025)155

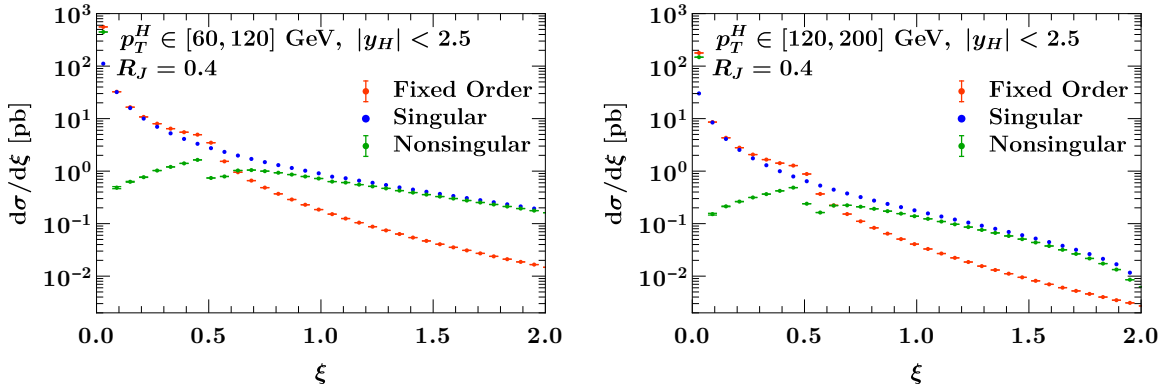

Figure 5. Decomposition of the full cross section (red) in terms of the singular (blue) and nonsingular (green) as function of $\xi = p_T^{\text{cut}}/p_T^H$. Our transition points are chosen on the basis of this plot. By using ξ, this is fairly independent of the hard kinematics, as can be seen by comparing the left ($p_T^H \in [60, 120]$ GeV) and right ($p_T^H \in [120, 200]$ GeV) panel.

enabling a smooth transition of the scales in eq. (3.61) to the common scale μ_{FO} in the fixed-order regime.

For a $2 \to 1$ process such as $gg \to H$, there is limited freedom in how one defines the transition parameter ξ due to the simple kinematic dependence of the hard scattering. For a $2 \to 2$ process, however, more possibilities arise — for example, far from the singular limit $p_T^J \neq p_T^H$ and ξ could depend on either quantity (or conceivably both). Given that we are interested in making predictions for p_T^H, we choose

$$\xi = \frac{p_T^{\text{cut}}}{p_T^H} \,. \tag{3.71}$$

We have verified that this choice ensures the points of transition are roughly independent of the phase space bin being considered. This is illustrated in figure 5 for two different bins of the hard scattering kinematics. We also use this plot to select the values of x_1, x_2, and x_3 which appear in eq. (3.70) and which are used to control precisely where and how quickly the scale merging occurs. We select the values $\{x_1, x_2, x_3\} = \{0.15, 0.4, 0.65\}$, which coincides with the choices made in ref. [16].

3.3.4 Fixed-order matching

Our NLL′ resummed predictions for the Higgs p_T^H spectrum in H+1-jet production are matched to fixed-order calculations obtained from GENEVA [70] at NLO_1 accuracy (where NLO_i denotes a next-to-leading order calculation with i partons in the final state). To match our approximate NNLL′ results consistently, we require a corresponding NNLO_1 calculation. Unfortunately, however, no publicly available code capable of producing such a prediction currently exists. We therefore reconstruct the NNLO_1 inclusive cross section as a function of p_T^H by taking the NLO_1 prediction from GENEVA with $p_T^{\text{cut}} \to \infty$ (retaining all rapidity cuts) and reweighting by a K-factor which is determined via examination of the results for the Higgs p_T^H spectrum at NNLO_1 shown in refs. [40, 41]. This is viable since with the

JHEP03(2025)155

fixed-order scale choice in eq. (3.64) (and also used in refs. [40, 41]) the NNLO_1 correction is approximately flat as a function of p_T^H in our region of interest. While the results in refs. [40, 41] do not include a cut on the Higgs rapidity, we have verified that the effect of placing a rapidity cut $|y_H| < 2.5$ has an almost identical effect on p_T^H at LO_1 and NLO_1. This allows us to use the NNLO_1 K-factor obtained from results which do not have this additional rapidity cut. We obtain a central value of $K_{\mathrm{NNLO}_1} = 1.25$.

From this inclusive NNLO_1 result we then subtract the contributions from the region of phase space where the transverse momentum of the second jet, p_T^{2nd}, is above our desired cut-off p_T^{cut},

$$\left.\frac{\mathrm{d}\sigma_{Hj}^{\mathrm{NNLO}}}{\mathrm{d}p_T^H}\right|_{p_T^{\mathrm{2nd}}<p_T^{\mathrm{cut}}} = K_{\mathrm{NNLO}_1}\left.\frac{\mathrm{d}\sigma_{Hj}^{\mathrm{NLO}}}{\mathrm{d}p_T^H}\right|_{p_T^{\mathrm{cut}}\to\infty} - \left.\frac{\mathrm{d}\sigma_{Hjj}^{\mathrm{NLO}}}{\mathrm{d}p_T^H}\right|_{p_T^{\mathrm{2nd}}>p_T^{\mathrm{cut}}}. \tag{3.72}$$

For distributions differential in p_T^H, this subtraction term (the NLO_2 cross section with $p_T^{\mathrm{2nd}} > p_T^{\mathrm{cut}}$) can be obtained directly from GENEVA by setting appropriate cuts on the second jet. This method allows us to reconstruct the NNLO_1 result down to values of $p_T^{\mathrm{cut}} > 10\,\mathrm{GeV}$.

3.4 Perturbative uncertainties and theory nuisance parameters

The theoretical uncertainties associated with our calculation have three distinct origins. The first relates to the fact that, at the order in resummed perturbation theory to which we are working, we have incomplete knowledge of the perturbative ingredients. We deal with this by introducing theory nuisance parameters [39], for which a central value is estimated and variations performed to assess the associated uncertainty due to the missing ingredient. The second source of uncertainty arises from the freedom we have in choosing how the resummation is turned off in transitioning to the fixed-order region of phase space. This "matching" uncertainty is associated with our choice of the parameters x_1, x_2, and x_3 in eq. (3.70). The third, more usual source is the lack of knowledge of terms which are of higher order in perturbation theory than the order to which we work and arise because of the truncation of the perturbative series in the first place. We first discuss how we quantify the latter uncertainties by varying the profile scales before moving on to provide a more detailed description of uncertainties from theory nuisance parameters.

3.4.1 Profile scale variations

As is usual, the contribution from missing higher order terms is estimated by a scale variation procedure. By independently varying the exact form of the profile functions μ_B, μ_S, μ_J, $\mu_{\mathcal{S}}$, ν_S, ν_B in eqs. (3.67) and (3.68) while keeping the scale μ_H fixed, we alter the arguments of the logarithms being resummed and hence obtain a resummation uncertainty. This probes the intrinsic uncertainty in the resummed logarithmic series. It is important, however, that the uncertainties generated from these scale variations are gradually turned off in the same manner as the resummation as one enters the fixed-order region of phase space.

The profile scale variations and how they are shut off are controlled by the parameters $V_X, W_Y \in \{0, 1, -1\}$ and $f_{\mathrm{vary}}(\xi)$ in eqs. (3.67) and (3.68) where

$$f_{\mathrm{vary}}(x) = \begin{cases} 2\left(1 - \frac{x^2}{x_3^2}\right) & 0 \le x < \frac{x_3}{2}\,, \\ 1 + 2\left(1 - \frac{x}{x_3}\right)^2 & \frac{x_3}{2} \le x < x_3\,, \\ 1 & x_3 \le x\,. \end{cases} \tag{3.73}$$

JHEP03(2025)155

Thus $f_{\text{vary}}(\xi)$ runs from 2 in the resummation region to 1 in the fixed-order region and acts as a multiplier of the scales around their central values, while V_X and W_Y control whether the variation is by a factor of 2 or 1/2 (or not at all). Our procedure for varying the scales follows that in section III.C of ref. [16] and we outline it only briefly here. We highlight that varying each of the six scales μ_B, μ_S, μ_J, $\mu_{\mathcal{S}}$, ν_S, ν_B independently through all possible combinations is undesirable, since it can lead to combinations which alter the arguments of logarithms by factors of four rather than two (such as the combination $\{2\nu_B, \nu_S/2\}$ for logarithms containing the ratio ν_B/ν_S). To avoid such situations we omit simultaneous scale variations which would lead to these factors of four. Furthermore, we vary the scales in the global soft and soft-collinear functions simultaneously by the same factor (though their central values are of course different). Our factorization of the total soft function into global and soft-collinear functions as outlined in section 3.1.4 already introduces a number of nuisance parameters. Keeping their scale variations consistent avoids double counting the associated resummation uncertainty.

In summary, we impose the following conditions

$$V_S = V_{\mathcal{S}}\,, \quad V_S V_B \geqslant 0\,, \quad W_S W_B \geqslant 0\,, \quad V_S W_S \geqslant 0\,, \tag{3.74}$$

where the last three conditions avoid generating factors of four in logarithms containing ratios of μ_S/μ_B, ν_S/ν_B, and μ_S/ν_S respectively. This results in 122 separate variation combinations to consider. The resulting uncertainty is then given by constructing a symmetric envelope using the points which produce the largest magnitude of deviation across all variations, resulting in the resummation uncertainty Δ_{resum}.

In addition to these individual scale variations, we collectively vary all scales up and down. At large p_T^{cut} this corresponds to the normal procedure followed in a fixed-order calculation, while at small p_T^{cut} it preserves the arguments of all logarithms being resummed. We therefore refer to this as a fixed-order variation and it is achieved through the choice of $V_{\text{FO}} \in \{0, 1, -1\}$ in eq. (3.65), which feeds into μ_H via eq. (3.66) and all other scales via eqs. (3.67) and (3.68). This produces only two new variations in addition to the central curve — we again symmetrize by taking the maximum deviation to produce an uncertainty Δ_{FO}. When performing these variations we also consistently vary the scales entering in the nonsingular, adjusting the NNLO_1 K-factor appropriately. This ensures that we correctly reproduce the scale variation bands of the inclusive NNLO_1 calculation given in refs. [40, 41].

The second source of uncertainty introduced at the start of this section originates from the arbitrariness in choosing the transition points x_i which define the shape of the profile. Our central choice for these parameters is given by $\{x_1, x_2, x_3\} = \{0.15, 0.4, 0.65\}$ as discussed at the end of section 3.3.3, while variations from this are given by

$$\{x_1, x_2, x_3\} = \{\{0.1, 0.35, 0.6\}, \{0.1, 0.4, 0.7\}, \{0.2, 0.4, 0.6\}, \{0.2, 0.45, 0.7\}\}\,. \tag{3.75}$$

This corresponds to moving all transition points to larger and smaller values by 0.05, as well as keeping the centre of the transition fixed and moving the start and end points simultaneously closer or further away from the central point again by 0.05. The symmetrized envelope results in the matching uncertainty Δ_{match}.

JHEP03(2025)155

3.4.2 Theory nuisance parameters

We now move on to discuss the parameterization of missing terms at the perturbative order to which we are working using theory nuisance parameters (TNPs) [39]. The unknown ingredients include both two-loop anomalous dimensions and also NNLO constant (nonlogarithmic) terms. In section 3.3.1, we obtained all anomalous dimensions from consistency relations with one exception — the split between the two-loop noncusp anomalous dimensions for the global soft and soft-collinear functions. We manifest our ignorance by introducing a TNP θ_1 as

$$\gamma^j_{\mathcal{S}\,1} \propto C_j\,\theta_1\,, \tag{3.76}$$

and obtain the two-loop coefficient of the global soft anomalous dimension from the difference $\gamma^\kappa_{S\,1} = \gamma^\kappa_{S,T\,1} - \gamma^j_{\mathcal{S}\,1}$. We thus need only one TNP for the remaining missing anomalous dimensions.

A priori, we have a total of 6 unknown two-loop constant terms, namely

$$j_g^{(2)},\ s_{ggg}^{(2)},\ s_{qgq}^{(2)},\ s_{q\bar{q}g}^{(2)},\ s_g^{R,(2)},\ s_q^{R,(2)}\,. \tag{3.77}$$

If we assume Casimir scaling for the soft and soft-collinear constants and also neglect any possible R_{cut} dependence in them, this can be reduced to three unknowns. We therefore introduce three more TNPs,

$$j_g^{(2)} \propto \theta_2\,, \qquad s_\kappa^{(2)} \propto (C_a + C_b + C_j)\,\theta_3\,, \qquad s_i^{R,(2)} \propto C_i\,\theta_4\,, \tag{3.78}$$

where the proportionality symbol again reminds us that we have a certain amount of freedom in how we choose the central values (and does not necessarily imply strict proportionality). We are thus left with a total of four parameters θ_{1-4}.

It is worth noting that in principle the two-loop soft constant $s_\kappa^{(2)}$ may be a function of the Born kinematics of the process as well as the jet radius. One could therefore consider introducing further TNPs to parameterize these dependences to capture correlations in them. Since, however, we only consider one value of the jet radius and a single rapidity bin, this is unnecessary in our case and we are able to treat these terms as effective constants. For a further discussion see ref. [39].

Having identified the role played by each nuisance parameter, we are able to make some educated guesses about the relations in eqs. (3.76) and (3.78) based on the structure of each of the missing terms. For $\gamma^j_{\mathcal{S}}$, we pick the central value to correspond to the known two-loop noncusp anomalous dimension for the hemisphere soft function appearing in the resummation of thrust (see eq. (3.56) of ref. [73]) and write

$$\gamma^j_{\mathcal{S}\,1} = -16 C_j \left[C_A \left(-\frac{101}{54} + \frac{11}{144}\pi^2 + \frac{7}{4}\zeta_3 \right) + T_F n_f \left(\frac{14}{27} - \frac{\pi^2}{36} \right) \right] \theta_1\,. \tag{3.79}$$

This can (only) be expected to give the correct typical size of $\gamma^j_{\mathcal{S}}$. We therefore take as the central value $\theta_1 = 1$ and vary it by ± 1, as shown along with the other TNPs in table 3.

For $j_g^{(2)}$ we pick the central value by Casimir scaling with respect to the known expression in the quark case, $j_q^{(2)}$,

$$j_g^{(2)} = 4 C_A (-1.78\,C_F - 106.87\,C_A + 14.072\,T_F n_f)\theta_2\,. \tag{3.80}$$

JHEP03(2025)155

This can again be expected to give the correct typical size (but only that), which we have checked at one loop and also for other jet functions that are known at two loops for both quarks and gluons. We therefore take the central value to be $\theta_2 = 1$ and vary it by ± 1.

The two remaining unknowns relate to constant terms in the NNLO soft functions. Since these are given by correlators of Wilson lines related to the external partons, we parametrize both functions by assuming each is related to products of single Wilson lines, which in particular allows us to obtain the appropriate Casimir scaling for the leading overall colour factor. Specifically, if we parametrize the contribution to the constant term in a soft function from a single Wilson line associated to parton i as

$$Y_i = 1 + \frac{\alpha_s}{4\pi} C_i Y^{(1)} + \left(\frac{\alpha_s}{4\pi}\right)^2 C_i C_A Y^{(2)} + \cdots , \tag{3.81}$$

then we can model the constant terms in the global soft function as

$$\begin{aligned} s_\kappa \approx Y_a Y_b Y_j = 1 &+ \frac{\alpha_s}{4\pi}(C_a + C_b + C_j) Y^{(1)} \\ &+ \left(\frac{\alpha_s}{4\pi}\right)^2 \left[(C_a C_b + C_a C_j + C_b C_j)\big(Y^{(1)}\big)^2 + C_A (C_a + C_b + C_j) Y^{(2)}\right] . \end{aligned} \tag{3.82}$$

The entire α_s^2 term comprises our unknown $s_\kappa^{(2)}$ term, but constructing it in this manner gives us an expected known piece related to the square of the one-loop term $s_\kappa^{(1)}$ term. Matching the known NLO term requires that $Y^{(1)} = -\frac{\pi^2}{6}$. Substituting this in the $\mathcal{O}(\alpha_s^2)$ term we finally parametrize the unknown $s_\kappa^{(2)}$ as

$$s_\kappa^{(2)} = (C_a C_b + C_a C_j + C_b C_j)\frac{\pi^4}{36} + 16\, C_A (C_a + C_b + C_j)\theta_3 , \tag{3.83}$$

where we have replaced $Y^{(2)}$ by $16\theta_3$. With this normalization convention, the missing two-loop term can be expected to be of size $|\theta_3| \lesssim 1$ [39]. Having no prior expectation of the sign of this term, we set the central value to $\theta_3 = 0$ and vary it (conservatively) by ± 2.

An analogous analysis for the missing two-loop constant for the soft-collinear function yields

$$s_i^{R,(2)} = \frac{\pi^4}{36} C_j^2 + 32\, C_A C_j \theta_4 , \tag{3.84}$$

where as for θ_3 we take $\theta_4 = 0 \pm 2$.

The uncertainty associated with these unknowns is quantified by varying the θ_i independently, one-at-a-time, around their central values by $\pm\Delta\theta_i$ as summarized in table 3. The TNPs we use are associated solely with unknown parts of the resummed calculation, while the fixed-order piece is, in principle, known exactly. It would therefore be undesirable to continue to vary them in the fixed-order region dominated by the fixed-order calculation, since this would result in an overestimate of the theoretical uncertainty. To avoid this, when performing the fixed-order matching we gradually shut off the TNP variation as a function of $\xi = p_T^{\text{cut}}/p_T^H$, using the same function g_{run} defined in eq. (3.70),

$$\theta_i = \theta_i^{\text{central}} \pm \Delta\theta_i\, g_{\text{run}}(\xi) . \tag{3.85}$$

JHEP03(2025)155

	Central	Upper	Lower
θ_1	1	2	0
θ_2	1	2	0
θ_3	0	2	−2
θ_4	0	2	−2

Table 3. Central values and variations used for the theory nuisance parameters.

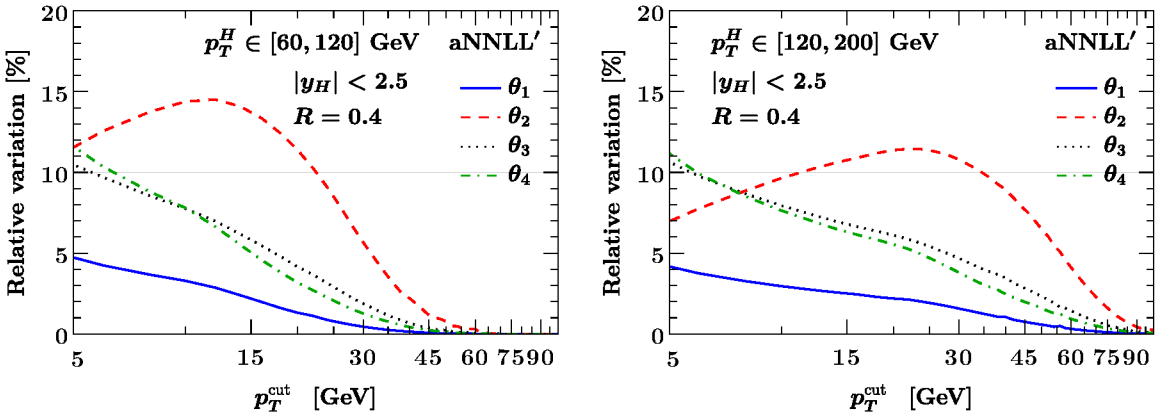

Figure 6. Relative uncertainty from varying each theory nuisance parameter as a function of p_T^{cut} for two different STXS bins.

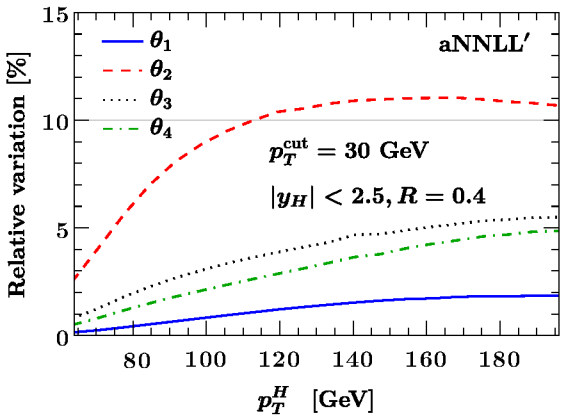

Figure 7. Relative uncertainty from varying each theory nuisance parameter for the p_T^H spectrum with a jet veto at $p_T^{\text{cut}} = 30\,\text{GeV}$.

In so doing, we ensure that the TNP variation is switched off in exactly the same way as the resummation itself. The uncertainty due to each TNP is again taken as the maximum absolute deviation between the up and down variations. Since each TNP parametrizes an uncorrelated source of uncertainty, their resulting individual uncertainties are added in quadrature to give a combined uncertainty estimate Δ_{TNP}.

JHEP03(2025)155

In figures 6 and 7 we show the relative impact due to the variation of each TNP for the $p_T^{\rm cut}$ cumulant and p_T^H distributions. It is clear that θ_2 (associated with the unknown two-loop constant term in the gluon jet function) has the biggest impact, though θ_3 and θ_4 (which are associated with the missing two-loop constant terms in the global soft and soft-collinear functions) give increasing contributions as $p_T^{\rm cut}$ decreases. The uncertainties associated with θ_3 and θ_4, while still less than θ_2, grow as a function of p_T^H for fixed $p_T^{\rm cut}$.

One possible reason for the relatively large uncertainty generated by θ_2 compared to say θ_3 or θ_4, which also represent unknown two-loop constant contributions, is the very large numerical value of $j_q^{(2)}$ on which our estimate of $j_g^{(2)}$ is based. The expression in eq. (3.80) evaluates to

$$j_g^{(2)} = -3453.64\,\theta_2\,. \tag{3.86}$$

The expressions for $s_\kappa^{(2)}$ and $s_i^{R,(2)}$ in eqs. (3.83) and (3.84) evaluate in the gluon-gluon channel to

$$s_{ggg}^{(2)} = 73.06 + 432\,\theta_3 \quad \text{and} \quad s_g^{R,(2)} = 24.35 + 288\,\theta_4\,. \tag{3.87}$$

Although $j_g^{(2)}$ only enters in contributions with a final state gluon and the soft terms will enter in all channels, the large numerical hierarchy between them for the gluon-gluon channel could already point to a reason for the significant difference in the uncertainty generated through variation of the associated TNPs.

The various sources of uncertainty Δ_i discussed in this section are combined in quadrature to obtain the final uncertainty estimate,

$$\Delta_{\rm total} = \sqrt{\Delta_{\rm FO}^2 + \Delta_{\rm resum}^2 + \Delta_{\rm match}^2 + \Delta_{\rm TNP}^2}\,. \tag{3.88}$$

The uncertainty bands of a given distribution are then generated by $\mathrm{d}\sigma(x) \pm \Delta_{\rm total}(x)$ for $x \in \{p_T^{\rm cut}, p_T^H\}$ depending on the distribution under consideration and $\mathrm{d}\sigma(x)$ represents the central curve. All our results are shown with uncertainties generated in this manner (where $\Delta_{\rm TNP} = 0$ for results to NLL and NLL′ accuracy).

4 Numerical results

In this section we present our numerical results. In the first set of plots we study the dependence on the jet veto for the two STXS 1-jet bins with $p_T^H \in [60, 120]\,\text{GeV}$ and $p_T^H \in [120, 200]\,\text{GeV}$. In the second set of plots we explore the dependence on p_T^H for a fixed value of the jet veto $p_T^{\rm cut} = 30\,\text{GeV}$. We always include a cut on the Higgs rapidity $|y_H| \leq 2.5$. For the jet radius we always use $R_J = R_{\rm cut} = R = 0.4$. We always work at $E_{\rm cm} = 13\,\text{TeV}$ using the `MSHT20nnlo` PDFs with $\alpha_s(m_Z) = 0.118$ [74].

In figure 8 we show the convergence of the pure resummed results, comparing NLL, NLL′ and aNNLL′ for the two STXS bins. In the resummation region (small $p_T^{\rm cut}$), the uncertainty bands overlap well and decrease in size at higher orders, indicating that resummed perturbation theory is well behaved. Despite the fact that not all of the resummation ingredients at NNLL′ are known, the approximate aNNLL′ results still provide a substantial improvement compared

JHEP03(2025)155

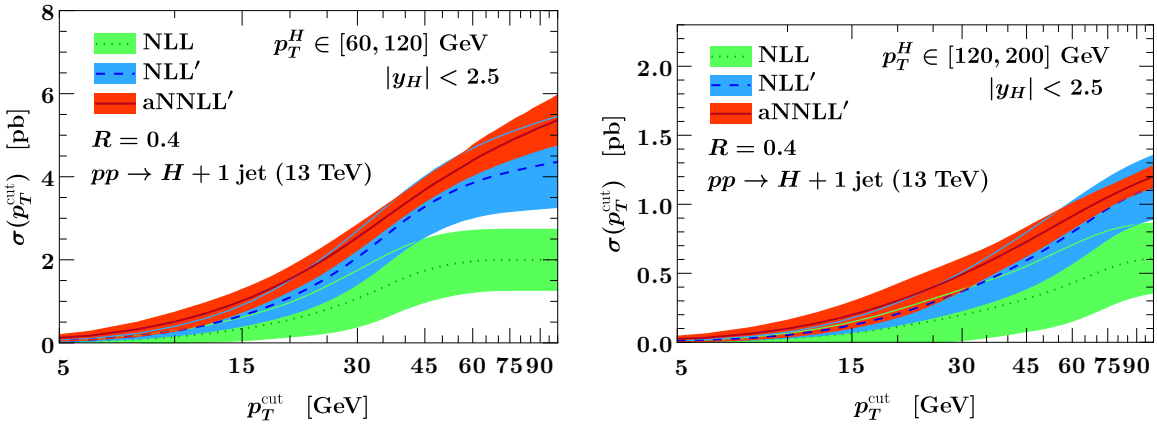

Figure 8. Convergence of resummed perturbation theory as function of $p_T^{\rm cut}$, comparing NLL (green dotted), NLL′ (blue dashed) and aNNLL′ (red solid) for two different STXS bins. The uncertainty bands are obtained as described in section 3.4.

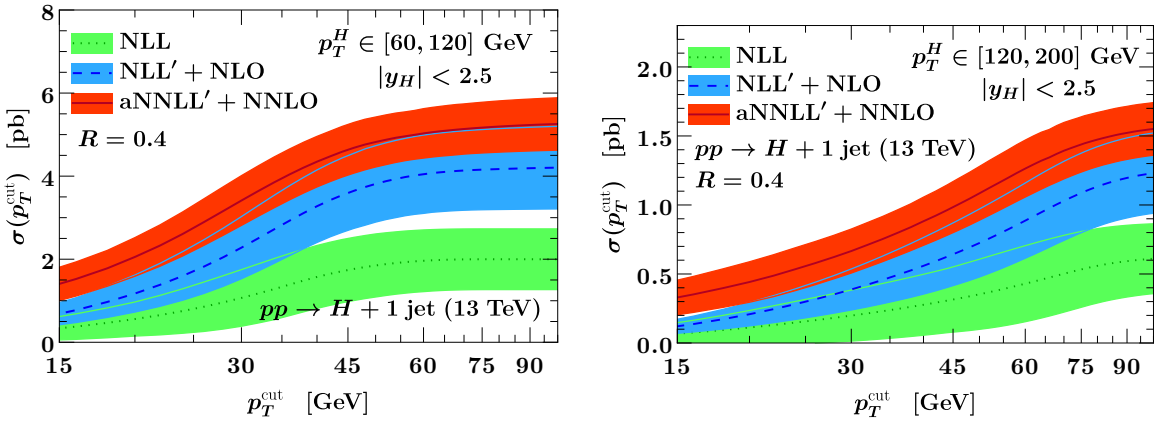

Figure 9. Same as figure 8 but including the matching to fixed-order perturbation theory.

to the previous NLL′ order. For the STXS bin with small p_T^H (left panel) there is a gap between the NLL band and the others for large values of $p_T^{\rm cut}$. This is of no concern, as this is the fixed-order region where the matching to fixed order becomes necessary.

This brings us to figure 9, where compared to figure 8 the fixed-order matching is included. Including the nonsingular contribution increases the uncertainty band of the cross section. Nonetheless, the relative uncertainty at aNNLL′+NNLO compared to NLL′+NLO still shows a noticeable reduction. Explicit numerical results for two representative $p_T^{\rm cut}$ values are given in table 4. The gap between the NLL and other orders for large values of $p_T^{\rm cut}$ seen in the left panel of figure 8 becomes worse when the matching is included. This is again not a feature of our resummed calculation, but rather of the underlying inclusive Higgs+jet fixed-order cross section, for which it is known that the scale variations do not cover the increase from LO to NLO (see e.g. refs. [40, 41]).

JHEP03(2025)155

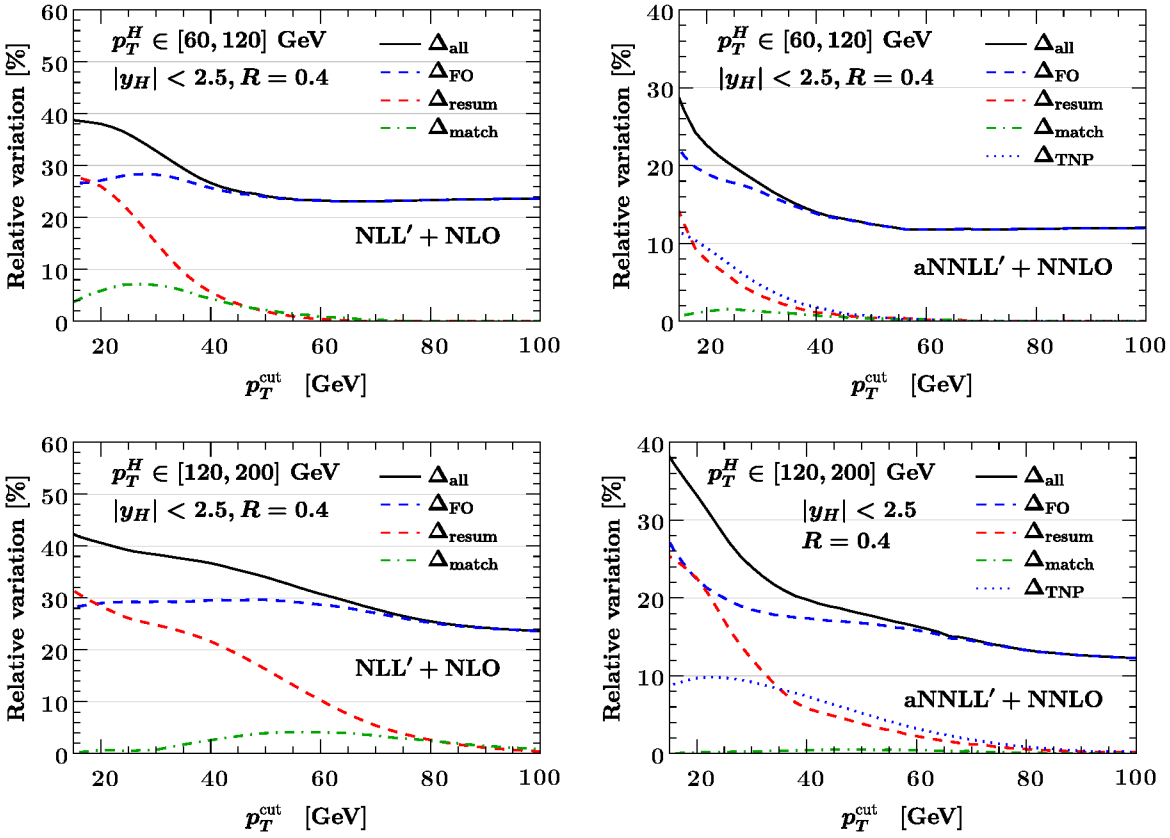

Figure 10. Breakdown of the total perturbative uncertainty as function of p_T^{cut} for the low p_T^H bin (top row) and the high p_T^H bin (bottom row). For each bin, the uncertainties at NLL′+NLO (left) and aNNLL′+NNLO (right) are given. The relative uncertainties from the individual uncertainty sources as discussed in section 3.4 are shown in blue dashed (fixed-order), red dashed (resummation), and green dashed (matching). At aNNLL′, the uncertainty due to TNPs is shown by the blue dotted curve. The total uncertainty (solid black) is obtained by adding these in quadrature.

In figure 10 we show a detailed breakdown of the various contributions to our uncertainties at NLL′+NLO and aNNLL′+NNLO for the two STXS bins. As expected, for large values of p_T^{cut}, the uncertainty is simply the fixed-order uncertainty. For small values of p_T^{cut} the uncertainty from resummation becomes larger and of similar size to the fixed-order uncertainty at NLL′+NLO. At aNNLL′+NNLO, the fixed-order uncertainty also grows for small values of p_T^{cut} staying dominant for low p_T^H and on par with the resummation uncertainty for the high p_T^H STXS bin. The uncertainty from the matching procedure, governing the transition between the resummed and fixed-order calculation, is negligible compared to the other uncertainties. At aNNLL′+NNLO, there is also an uncertainty due to the TNPs. Its contribution is roughly on par with the resummation uncertainty for the small p_T^H bin. For the high p_T^H bin the TNP uncertainty tracks the resummation uncertainty for values of $p_T^{\text{cut}} > 35\,\text{GeV}$ but then levels off at around 10% for low p_T^{cut} while the resummation uncertainty continues to grow.

We next compare our best result at aNNLL′+NNLO to the fixed NNLO prediction in figure 11. Here, the uncertainty at fixed NNLO is obtained using the ST method [75]

JHEP03(2025)155

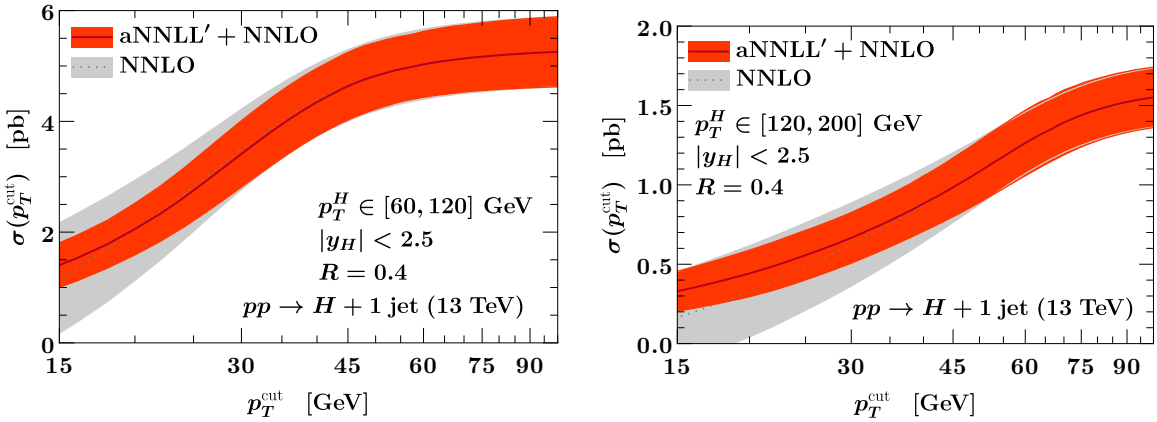

Figure 11. Comparison of our aNNLL′+NNLO prediction (red) to NNLO (grey dotted) as function of $p_T^{\rm cut}$, showing the reduction in uncertainty from the resummation. The uncertainty band on our prediction is obtained using the method described in section 3.4, while the ST method is used for the uncertainty at fixed NNLO.

	Cross section [pb]			
STXS bin	$p_T^H \in [60, 120]$ GeV		$p_T^H \in [120, 200]$ GeV	
$p_T^{\rm cut}$ [GeV]	20	30	20	30
NNLO	$2.03 \pm 44\%$	$3.49 \pm 21\%$	$0.329 \pm 87\%$	$0.624 \pm 42\%$
NLL	$0.56 \pm 73\%$	$1.07 \pm 64\%$	$0.112 \pm 110\%$	$0.198 \pm 93\%$
NLL′+NLO	$1.17 \pm 38\%$	$2.28 \pm 33\%$	$0.209 \pm 41\%$	$0.388 \pm 38\%$
aNNLL′+NNLO	$2.05 \pm 23\%$	$3.41 \pm 18\%$	$0.442 \pm 33\%$	$0.666 \pm 24\%$

Table 4. Sample numerical values for our resummed predictions. Both STXS bins use a cut $|y_H| < 2.5$. The uncertainties correspond to the total uncertainty according to eq. (3.88) for the resummed results and to the ST uncertainties [75] for the NNLO results.

(which is commonly used in this context to avoid artificially small scale variations due to accidental cancellation between the large K factor of the inclusive cross section and the large jet-veto logarithms). As expected, these predictions coincide for large values of $p_T^{\rm cut}$, but the uncertainty of our resummed prediction becomes smaller than at fixed NNLO as $p_T^{\rm cut}$ decreases. The improvement from resummation is more pronounced for the STXS bin in the right panel, since for fixed $p_T^{\rm cut}$ the resummed logarithms increase with increasing p_T^H. The explicit numerical results for the two STXS bins at $p_T^{\rm cut} = 20\,\text{GeV}$ and $p_T^{\rm cut} = 30\,\text{GeV}$ are given in table 4. The uncertainties given correspond to the total uncertainty in eq. (3.88) for the resummed results and the ST uncertainties for the fixed NNLO results. It should be noted that the individual sources of uncertainty between the two STXS bins should be considered correlated.

In the following set of plots we repeat the above results but explore the dependence on p_T^H while keeping $p_T^{\rm cut} = 30\,\text{GeV}$ fixed. In the left panel of figure 12, we show the analogue of figure 9. We remind the reader that we work in the heavy-top approximation, and that for

JHEP03(2025)155

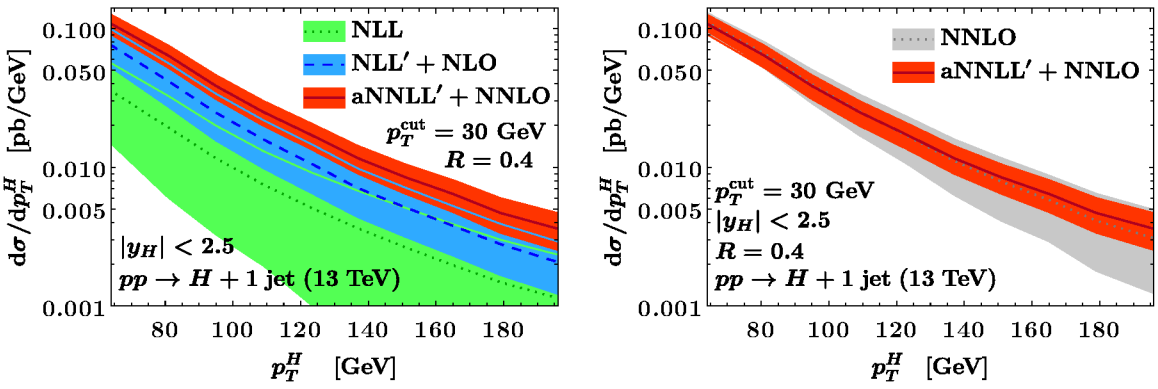

Figure 12. Left panel: the convergence of resummed perturbation theory as function of p_T^H, comparing NLL (green dotted), NLL′+NLO (blue dashed), and aNNLL′+NNLO (red solid) for $p_T^{\rm cut} = 30\,\text{GeV}$, $|y_H| < 2.5$ and $R_J = 0.4$. The uncertainty bands are obtained using the method described in section 3.4. Right panel: comparison of our aNNLL′+NNLO prediction (red) to NNLO (grey dotted) as function of p_T^H for $p_T^{\rm cut} = 30\,\text{GeV}$. The uncertainty on the NNLO is obtained using the ST method.

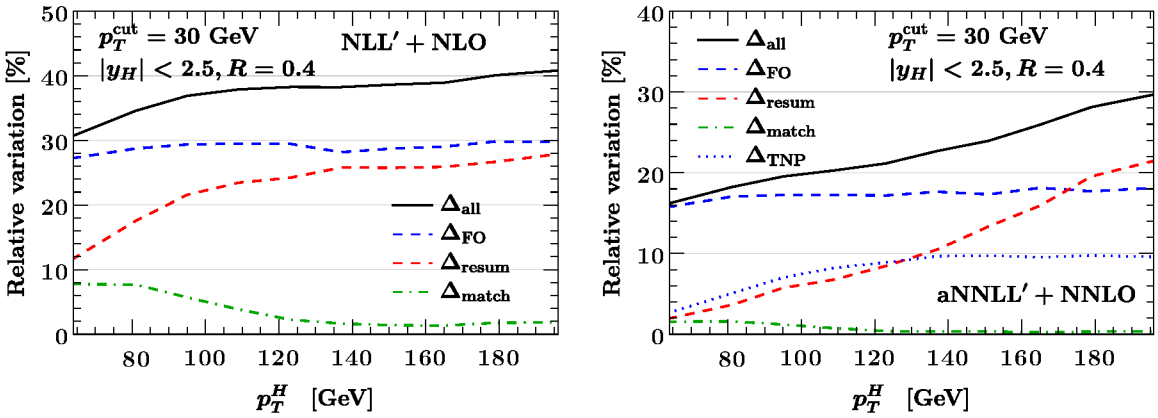

Figure 13. Same as figure 10 but as function of p_T^H for fixed $p_T^{\rm cut} = 30\,\text{GeV}$.

$p_T^H > 200\,\text{GeV}$ finite top-quark mass effects become relevant [76, 77]. The overlapping bands and reduction of the bands at higher orders highlight the good convergence of resummed perturbation theory for the nominal value of the jet veto. In the right panel, we compare our aNNLL′+NNLO to the NNLO result. For small values of p_T^H, the hierarchy between $p_T^{\rm cut}$ and p_T^H reduces so we are effectively leaving the resummation region and approach the fixed-order region. Hence, the resummed and fixed-order results become equal. In contrast, for larger values of p_T^H we are going deeper into the resummation region and the uncertainty on the aNNLL′+NNLO prediction reduces by a factor of 2 or more compared to the NNLO prediction. Finally, in figure 13 we show the breakdown of the uncertainty as function of p_T^H for fixed $p_T^{\rm cut} = 30\,\text{GeV}$ analogous to figure 10. As expected, as p_T^H increases the resummation and TNP uncertainties increase while the matching uncertainty decreases.

JHEP03(2025)155

5 Conclusions

In this work, we have provided state-of-the-art predictions for Higgs boson production in the exclusive 1-jet bin. Demanding exactly one hard jet requires the introduction of a veto scale, which in turn causes large logarithms of the ratio of that scale to the natural hard scale of the process to arise in the perturbative calculation. We have resummed these large logarithms to all orders in α_s using the framework of Soft-Collinear Effective Theory, extending a factorization formula first developed in ref. [36], and matched our results to a calculation at fixed order in perturbation theory.

Our work has several novel features which provide important improvements over previous studies. First, we extend the formal accuracy to NNLL$'$ for the resummed component and push the fixed order part to NNLO using the numerical results of refs. [40, 41]. Though the lack of some of the requisite two-loop ingredients only allows us to reach an approximate NNLL$'$ accuracy in practice, we are able to quantify the additional perturbative uncertainty associated with these missing terms by variation of appropriately defined theory nuisance parameters. The total perturbative uncertainty is still significantly improved compared to NLL$'$. Second, we perform a refactorization of the soft sector which allows logarithms of the signal jet radius R_J to be resummed. This is achieved using a SCET$_+$ formalism, in which an additional soft-collinear mode is introduced. Third, we study the effect of power corrections in R_J on the soft function which multiply logarithms of p_T^{cut}. We have found that the inclusion of these power corrections is necessary to recover the correct singular behaviour in the small p_T^{cut} limit, and that they in fact have a sizeable numerical effect in this region for phenomenologically relevant values of the jet radius $R_J \sim 0.4$. Fourth, we include in an approximate form the effect of nonglobal logarithms. By exploiting a five-loop solution of the BMS equation which resums these terms at leading logarithmic order, we are able to include these subleading effects into our factorisation formula.

Our work can be extended in various ways. Most obviously, a full knowledge of the two-loop soft, soft-collinear and gluon jet functions would allow to further reduce the perturbative uncertainties pushing the formal accuracy to full NNLL$'$. Such a resummation (possibly also including the effects of nonglobal logarithms to higher orders) could then be used as the basis of an event generator matching NNLO calculations for H+jet to parton showers, in the same vein as ref. [33]. It would also be interesting to obtain resummed predictions for the STXS 1-jet bin at low $p_T^H < 60\,\text{GeV}$. This scenario requires, however, a substantially different treatment, since the hierarchy of energy scales is altered. A suitable factorization formula for this setup still needs to be derived, likely necessitating the introduction of additional csoft modes in SCET$_+$. The work here can also be applied to the STXS 1-jet bins in VH production. It would also be fairly straightforward to include the Higgs decay and cuts on the decay products to obtain fully fiducial predictions for exclusive H+1-jet production. Our approach could also be extended to cases with additional hard jets in the final state. This would not entail any changes to the collinear components of our calculation, but the hard function would need to be extracted from the (known) two-loop amplitudes and the relevant soft functions would need to be computed. In addition, this would introduce nontrivial colour structure to the resummation, which could be dealt with in a manner similar to that employed in e.g. refs. [78–80].

JHEP03(2025)155

Acknowledgments

We are grateful to Piotr Pietrulewicz for early collaboration and to Simone Alioli for access to computing resources necessary for this work. MAL is indebted to Michael Penn, whose YouTube videos on logarithmic-trigonometric integrals were useful in the computation of the 1-loop soft function. This project has received funding from the European Research Council (ERC) under the European Union's Horizon 2020 research and innovation programme (Grant agreement 101002090 COLORFREE). MAL is supported by the UKRI guarantee scheme for the Marie Skłodowska-Curie postdoctoral fellowship, grant ref. EP/X021416/1.

A Clustering of collinear and soft-collinear emissions

A potential obstacle to the factorization in eq. (2.15) could be the clustering of jet-collinear and soft-collinear emissions. In this appendix, we demonstrate that this effect is in fact suppressed and contributes at the same order as subleading nonglobal logarithms, that is at $\mathcal{O}(\alpha_s^2 \ln(p_T^J/p_T^{\rm cut}))$.

We start by observing that we only have to concern ourselves with the effect of collinear emissions on the soft-collinear clustering, as soft-collinear emissions do not change the collinear clustering because they are much softer. If the jet consists of a single jet-collinear particle, the phase-space restriction of a soft-collinear emission is a fixed circle in (η, ϕ) with radius R_J. The effect of an additional jet-collinear emission is to shift the boundary, increasing the effective value of the radius $R_J \to kR_J$ (where $k \sim \mathcal{O}(1)$). The double logarithmic term appearing in the soft collinear function $L_R^2 = \ln^2(\mu/(p_T^{\rm cut} R_J))$ is then modified as

$$L_R^2 \to L_R^2 - 2L_R \ln k + \ln^2 k\,, \tag{A.1}$$

inducing a change in the single logarithmic term. Since the effect is due to mixing between jet-collinear and soft-collinear sectors, we take $\mu = p_T^J R_J$ and find that the contribution of this clustering effect on the cross section is $\propto \alpha_s^2 \ln(p_T^J/p_T^{\rm cut})$.

We still need to demonstrate that the integration over the phase space of the additional jet-collinear emission does not generate any further logarithms, otherwise the clustering could contribute at the same order as the leading nonglobal logarithms, which we do include. Concretely, we wish to show that, since the entire effect is given by a product of the one-loop jet and soft-collinear functions, the contribution from the jet function in the relevant phase space is a constant factor.

The condition that both jet-collinear emissions are clustered into one jet leads to the following restriction

$$s \leq z(1-z)(p_T^J R_J)^2 \tag{A.2}$$

where s is their invariant mass and z the momentum fraction. The clustering effect described above only occurs when the distance between the most energetic of the two collinear particles and the jet boundary is smaller than the distance between the two collinear particles. The reason is that the most energetic particle will be clustered first, and the problematic effect only occurs if the first clustering is with a soft-collinear emission. For simplicity we may

JHEP03(2025)155

consider $z < 1/2$ (the case $z > 1/2$ is equivalent by considering $z \to 1-z$), in which case the condition for clustering to occur is given by

$$R_J - \sqrt{\frac{zs}{(1-z)(p_T^J)^2}} < \sqrt{\frac{s}{z(1-z)(p_T^J)^2}} \tag{A.3}$$

with solution

$$s > \frac{z(1-z)}{(1+z)^2}(p_T^J R_J)^2 \,. \tag{A.4}$$

Eqs. (A.2) and (A.4) and $z < 1/2$ together determine the region of phase space $\mathcal{R}$ for which clustering occurs. Integrating over this region with a simplified integrand $1/(sz)$ is sufficient to capture the logarithmic structure. We find

$$\int_{\mathcal{R}} \frac{\mathrm{d}s}{s}\frac{\mathrm{d}z}{z} = -2\,\mathrm{Li}_2\left(-\frac{1}{2}\right) . \tag{A.5}$$

We observe that the integral is finite, and does not produce poles in ϵ (which when multiplying factors of $(p_T^J R_J)^\epsilon$ would generate further logarithms). We thus conclude that clustering of jet-collinear and soft-collinear emissions contributes at most an $\mathcal{O}\left(\alpha_s^2 \ln(p_T^J/p_T^{\mathrm{cut}})\right)$ effect.

B Calculation of the soft function at 1-loop

In this appendix, we revisit the calculation of the 1-loop soft function originally described in ref. [37]. We keep all logarithmic dependence on the jet radius R_J explicit throughout, anticipating the refactorization into a global-soft and soft-collinear function.

We begin with the expression for the soft current integrated over phase space, given by

$$S_\kappa = -\frac{2g_s^2}{(2\pi)^{d-1}}\left(\frac{e^{\gamma_E}\mu^2}{4\pi}\right)^\epsilon \sum_{\substack{l<m \\ l,m\in\kappa}} \mathbf{T}_l\cdot\mathbf{T}_m \int \mathrm{d}^d k\,\delta(k^2)\frac{n_l\cdot n_m}{(n_l\cdot k)(n_m\cdot k)}\,\mathcal{M}_s, \tag{B.1}$$

where $l, m = \{a, b, j\}$ and we are using the parametrization

$$\begin{aligned} k^\mu &= k_T(\cosh y, \ldots, \cos\phi, \sin\phi, \sinh y)\,, \\ n_a^\mu &= (1, \ldots, 0, 0, 1)\,, \\ n_b^\mu &= (1, \ldots, 0, 0, -1)\,, \\ n_j^\mu &= (\cosh y_J, \ldots, 1, 0, \sinh y_J)\,. \end{aligned} \tag{B.2}$$

The measurement function is given by

$$\mathcal{M}_{s,T}(k, p_T^{\mathrm{cut}}, R_J) = \Theta(p_T^{\mathrm{cut}} - k_T) + \Theta(k_T - p_T^{\mathrm{cut}})\Theta(R_J - \Delta R_{kJ})\,, \tag{B.3}$$

with $\Delta R_{kJ} = \sqrt{(y-y_J)^2+\phi^2}$. The first term on the r.h.s. is independent of the jet radius and contains all rapidity divergences, while the second contains the complete R_J dependence.

We may decompose the soft function according to colour structures, i.e.

$$S_\kappa^{(1)} = \mathbf{T}_a\cdot\mathbf{T}_b\,S_{ab} + \mathbf{T}_a\cdot\mathbf{T}_j\,S_{aj} + \mathbf{T}_b\cdot\mathbf{T}_j\,S_{bj}\,. \tag{B.4}$$

JHEP03(2025)155

We focus on the first term S_{ab} in eq. (B.4). Since this piece will suffer from rapidity divergences as $n_a \cdot k \to 0$ and $n_b \cdot k \to 0$, following ref. [37] we introduce a regulator of the form

$$|2k_3|^{-\eta}\nu^\eta \xrightarrow{|y|\to\infty} k_T^{-\eta}\nu^\eta \exp(-\eta\,|y|)\,. \tag{B.5}$$

It is sufficient to retain only the asymptotic behaviour of the regulator, since divergences occur only in this limit and elsewhere we can safely set $\eta = 0$. To leading order in R_J, we may expand $\Theta(R_J - \Delta R_{kJ}) = \mathcal{O}(R_J^2)$, yielding

$$\begin{aligned}
S_{ab} &= -\frac{g_s^2\Omega_{1-2\epsilon}}{2(2\pi)^{d-1}}\left(\frac{e^{\gamma_E}\mu^2}{4\pi}\right)^\epsilon \int \mathrm{d}y\mathrm{d}\phi\mathrm{d}k_T^2\,(k_T^2)^{-\epsilon-\eta/2}\nu^\eta e^{-\eta|y|}(\sin\phi)^{-2\epsilon}\,\frac{n_a\cdot n_b}{(n_a\cdot k)(n_b\cdot k)}\Theta(p_T^{\rm cut}-k_T)\\
&= \frac{2g_s^2\Omega_{2-2\epsilon}}{(2\pi)^{3-2\epsilon}}\left(\frac{e^{\gamma_E}}{4\pi}\right)^\epsilon \frac{2}{(2\epsilon+\eta)\eta}\left(\frac{\nu}{\mu}\right)^\eta\left(\frac{p_T^{\rm cut}}{\mu}\right)^{-2\epsilon-\eta}\\
&= \frac{\alpha_s}{4\pi}\left\{\frac{1}{\eta}\left[\frac{8}{\epsilon}+16\ln\left(\frac{\mu}{p_T^{\rm cut}}\right)\right]-\frac{4}{\epsilon^2}+\frac{8}{\epsilon}\ln\left(\frac{\nu}{\mu}\right)+8\ln^2\left(\frac{\mu}{p_T^{\rm cut}}\right)\ln\left(\frac{\nu}{\mu}\right)+16\ln\left(\frac{\mu}{p_T^{\rm cut}}\right)+\frac{\pi^2}{3}\right\}
\end{aligned} \tag{B.6}$$

We now turn to the computation of the S_{aj} contribution. The rapidity divergence at $n_a \cdot k \to 0$ is now regulated by

$$|2k_3|^{-\eta}\nu^\eta = 2^{-\eta}k_T^{-\eta}\nu^\eta|\sinh y|^{-\eta} \xrightarrow{y\to\infty} k_T^{-\eta}\nu^\eta\exp(-\eta\,y\,\Theta(y))\,. \tag{B.7}$$

We find

$$\begin{aligned}
S_{aj} &= -\frac{g_s^2\Omega_{1-2\epsilon}}{2(2\pi)^{d-1}}\left(\frac{e^{\gamma_E}\mu^2}{4\pi}\right)^\epsilon \int \mathrm{d}y\,\mathrm{d}\phi\,\mathrm{d}k_T^2\;(k_T^2)^{-\epsilon-\eta/2}\nu^\eta e^{-\eta\,y\,\Theta(y)}(\sin\phi)^{-2\epsilon}\,\frac{n_a\cdot n_J}{(n_a\cdot k)\,(n_J\cdot k)}\\
&\quad\times\Big[\Theta(p_T^{\rm cut}-k_T)+\Theta(R_J-\Delta R_{kJ})\Theta(k_T-p_T^{\rm cut})\Big]\\
&= -\frac{g_s^2\Omega_{1-2\epsilon}}{2(2\pi)^{3-2\epsilon}}\left(\frac{e^{\gamma_E}\mu^2}{4\pi}\right)^\epsilon \int \mathrm{d}\Delta y\,\mathrm{d}\phi\,\mathrm{d}k_T^2\;(k_T^2)^{-\epsilon-\eta/2}\nu^\eta e^{-\eta\,(\Delta y+y_J)\,\Theta(\Delta y+y_J)}(\sin\phi)^{-2\epsilon}\\
&\quad\times e^{\Delta y}\frac{1}{k_T^2(\cosh\Delta y-\cos\phi)}\Big[\Theta(p_T^{\rm cut}-k_T)+\Theta(R_J-\Delta R_{kJ})\Theta(k_T-p_T^{\rm cut})\Big]\\
&= \frac{g_s^2\Omega_{1-2\epsilon}}{(2\pi)^{3-2\epsilon}}\left(\frac{e^{\gamma_E}}{4\pi}\right)^\epsilon\frac{1}{2\epsilon+\eta}\left(\frac{\nu e^{-y_J}}{\mu}\right)^\eta\left(\frac{p_T^{\rm cut}}{\mu}\right)^{-2\epsilon-\eta}\\
&\quad\times\int \mathrm{d}\Delta y\,\mathrm{d}\phi\;e^{-\eta\,\Delta y\,\Theta(\Delta y)}(\sin\phi)^{-2\epsilon}\frac{e^{\Delta y}}{\cosh\Delta y-\cos\phi}\Theta(\Delta R_{kJ}-R_J),
\end{aligned} \tag{B.8}$$

where $\Delta y \equiv y - y_J$. In the above expression, the jet radius R_J serves to regulate a divergence associated with collinear emissions along the jet direction. Following ref. [37], we introduce the subtraction term

$$\mathcal{I}_R \equiv (\sin\phi)^{-2\epsilon}\,\frac{2\,e^{-\eta\Delta y\,\Theta(\Delta y)}}{\Delta y^2+\phi^2}\,, \tag{B.9}$$

which is obtained by taking the $R_J \to 0$ limit of the integrand of eq. (B.8). The $\ln R_J$ dependence of this subtraction term can be computed exactly, while the difference of the

subtraction term and the original integrand can be expanded in the limit $R_J \to 0$. We thus write

$$S_{aj} = \frac{g_s^2 \Omega_{1-2\epsilon}}{(2\pi)^{3-2\epsilon}} \left(\frac{e^{\gamma_E}}{4\pi}\right)^{\epsilon} \frac{1}{2\epsilon+\eta} \left(\frac{\nu e^{-y_J}}{\mu}\right)^{\eta} \left(\frac{p_T^{\text{cut}}}{\mu}\right)^{-2\epsilon-\eta} \times \left\{ \int \mathrm{d}\Delta y \, \mathrm{d}\phi \, (\sin\phi)^{-2\epsilon} e^{-\eta\,\Delta y\,\Theta(\Delta y)} \left[\frac{e^{\Delta y}}{\cosh\Delta y - \cos\phi} - \frac{2}{\Delta R_{kJ}^2}\right] \Theta(\Delta R_{kJ} - R_J) + \int \mathrm{d}\Delta y \, \mathrm{d}\phi \, (\sin\phi)^{-2\epsilon} \frac{2}{\Delta R_{kJ}^2} \Theta(\Delta R_{kJ} - R_J) \right\} \tag{B.10}$$

By replacing $\Theta(\Delta R_{kJ} - R_J) = 1 - \Theta(R_J - \Delta R_{kJ})$ in the last line of eq. (B.10), we may identify the integrals

$$S_{aj}^{\ln R_J} \equiv -\frac{g_s^2 \Omega_{1-2\epsilon}}{(2\pi)^{3-2\epsilon}} \left(\frac{e^{\gamma_E}}{4\pi}\right)^{\epsilon} \frac{1}{2\epsilon} \left(\frac{p_T^{\text{cut}}}{\mu}\right)^{-2\epsilon} \int_{-\infty}^{\infty} \mathrm{d}\Delta y \int_0^{\pi} \mathrm{d}\phi \sin\phi^{-2\epsilon} \frac{2}{\Delta R_{kJ}^2} \Theta(R_J - \Delta R_{kJ}) \tag{B.11}$$

$$S_{aj}^{\text{div}} \equiv \frac{g_s^2 \Omega_{1-2\epsilon}}{(2\pi)^{3-2\epsilon}} \left(\frac{e^{\gamma_E}}{4\pi}\right)^{\epsilon} \frac{1}{2\epsilon} \left(\frac{p_T^{\text{cut}}}{\mu}\right)^{-2\epsilon} \int_{-\infty}^{\infty} \mathrm{d}\Delta y \int_0^{\pi} \mathrm{d}\phi \sin\phi^{-2\epsilon} \frac{2}{\Delta R_{kJ}^2} \,. \tag{B.12}$$

We now take the small R_J limit: writing $\Delta y = \rho\cos\chi$ and $\phi = \rho\sin\chi$, we keep the leading term in the $\rho \to 0$ expansion. This amounts to making the replacement $(\sin\phi)^{-2\epsilon} \to \phi^{-2\epsilon}$ in eqs. (B.11) and (B.12). We thus have

$$S_{aj,R_J\to 0}^{\ln R_J} \equiv -\frac{g_s^2 \Omega_{1-2\epsilon}}{(2\pi)^{3-2\epsilon}} \left(\frac{e^{\gamma_E}}{4\pi}\right)^{\epsilon} \frac{1}{2\epsilon} \left(\frac{p_T^{\text{cut}}}{\mu}\right)^{-2\epsilon} \int_{-\infty}^{\infty} \mathrm{d}\Delta y \int_0^{\pi} \mathrm{d}\phi \, \phi^{-2\epsilon} \frac{2}{\Delta R_{kJ}^2} \Theta(R_J - \Delta R_{kJ}) \tag{B.13}$$

$$S_{aj,R_J\to 0}^{\text{div}} \equiv \frac{g_s^2 \Omega_{1-2\epsilon}}{(2\pi)^{3-2\epsilon}} \left(\frac{e^{\gamma_E}}{4\pi}\right)^{\epsilon} \frac{1}{2\epsilon} \left(\frac{p_T^{\text{cut}}}{\mu}\right)^{-2\epsilon} \int_{-\infty}^{\infty} \mathrm{d}\Delta y \int_0^{\pi} \mathrm{d}\phi \, \phi^{-2\epsilon} \frac{2}{\Delta R_{kJ}^2}. \tag{B.14}$$

In the first line of eq. (B.10), we may repeat the same tactic as before and introduce a further subtraction term to isolate the rapidity divergences of the integral for $\Delta y > 0$. We define

$$S_{aj}^{\eta} = \frac{g_s^2 \Omega_{1-2\epsilon}}{(2\pi)^{3-2\epsilon}} \left(\frac{e^{\gamma_E}}{4\pi}\right)^{\epsilon} \frac{1}{2\epsilon+\eta} \left(\frac{\nu e^{-y_J}}{\mu}\right)^{\eta} \left(\frac{p_T^{\text{cut}}}{\mu}\right)^{-2\epsilon-\eta} \int_{-\infty}^{\infty} \mathrm{d}\Delta y \int_0^{\pi} \mathrm{d}\phi \; 2(\sin\phi)^{-2\epsilon} e^{-\eta\,\Delta y} \times \Theta(\Delta y)\,\Theta(\Delta R_{kJ} - R_J) \tag{B.15}$$

$$S_{aj}^{\eta=0} = \frac{g_s^2 \Omega_{1-2\epsilon}}{(2\pi)^{3-2\epsilon}} \left(\frac{e^{\gamma_E}}{4\pi}\right)^{\epsilon} \frac{1}{2\epsilon} \left(\frac{p_T^{\text{cut}}}{\mu}\right)^{-2\epsilon} \int_{-\infty}^{\infty} \mathrm{d}\Delta y \int_0^{\pi} \mathrm{d}\phi \, (\sin\phi)^{-2\epsilon} \Theta(\Delta R_{kJ} - R_J) \times \left\{ e^{-\eta\,\Delta y} \left[\frac{e^{\Delta y}}{\cosh\Delta y - \cos\phi} - \frac{2}{\Delta R_{kJ}^2}\right] - 2\Theta(\Delta y) \right\}, \tag{B.16}$$

so that the whole expression in eq. (B.10) can be written as

$$S_{aj} = S_{aj}^{\ln R_J} + S_{aj}^{\text{div}} + S_{aj}^{\eta} + S_{aj}^{\eta=0} \,. \tag{B.17}$$

JHEP03(2025)155

Since eq. (B.16) is free of rapidity divergences, we may set the rapidity regulator $\eta = 0$ here. Again setting $\Theta(\Delta R_{kJ} - R_J) = 1 - \Theta(R_J - \Delta R_{kJ})$ in eqs. (B.15) and (B.16), the small R_J limit allows us to drop the second term in each case. We also recall that the second term in the square brackets of eq. (B.16) originates from eq. (B.11), which necessitates the replacement $(\sin\phi)^{-2\epsilon} \to \phi^{-2\epsilon}$. We obtain

$$S^{\eta}_{aj,R_J\to 0} = \frac{g_s^2\Omega_{1-2\epsilon}}{(2\pi)^{3-2\epsilon}}\left(\frac{e^{\gamma_E}}{4\pi}\right)^{\epsilon}\frac{1}{2\epsilon+\eta}\left(\frac{\nu e^{-y_J}}{\mu}\right)^{\eta}\left(\frac{p_T^{\text{cut}}}{\mu}\right)^{-2\epsilon-\eta}\int_{-\infty}^{\infty}\mathrm{d}\Delta y\int_0^{\pi}\mathrm{d}\phi \\ \times\, 2(\sin\phi)^{-2\epsilon}e^{-\eta\,\Delta y}\Theta(\Delta y) \tag{B.18}$$

$$S^{\eta=0}_{aj,R_J\to 0} = \frac{g_s^2\Omega_{1-2\epsilon}}{(2\pi)^{3-2\epsilon}}\left(\frac{e^{\gamma_E}}{4\pi}\right)^{\epsilon}\frac{1}{2\epsilon}\left(\frac{p_T^{\text{cut}}}{\mu}\right)^{-2\epsilon}\int_{-\infty}^{\infty}\mathrm{d}\Delta y\int_0^{\pi}\mathrm{d}\phi \\ \times\left\{\frac{e^{\Delta y}(\sin\phi)^{-2\epsilon}}{\cosh\Delta y-\cos\phi}-\frac{2\phi^{-2\epsilon}}{\Delta R_{kJ}^2}-2(\sin\phi)^{-2\epsilon}\Theta(\Delta y)\right\}. \tag{B.19}$$

Evaluating all integrals in the small R_J limit, we find

$$S^{\ln R_J}_{aj,R_J\to 0} = \frac{\alpha_s}{4\pi}\left[\frac{2}{\epsilon^2}+\frac{4}{\epsilon}\ln\left(\frac{\mu}{p_T^{\text{cut}}R_J}\right)+4\ln^2\left(\frac{\mu}{p_T^{\text{cut}}R_J}\right)-\frac{\pi^2}{6}\right], \tag{B.20}$$

$$S^{\text{div}}_{aj,R_J\to 0} = \frac{\alpha_s}{4\pi}\left[-\frac{2}{\epsilon^2}-\frac{4}{\epsilon}\ln\left(\frac{\mu}{2\pi p_T^{\text{cut}}}\right)-4\ln^2\left(\frac{\mu}{2\pi p_T^{\text{cut}}}\right)+\frac{\pi^2}{2}\right], \tag{B.21}$$

$$S^{\eta}_{aj,R_J\to 0} = \frac{\alpha_s}{4\pi}\left\{\frac{1}{\eta}\left[\frac{4}{\epsilon}+8\ln\left(\frac{\mu}{p_T^{\text{cut}}}\right)\right]-\frac{2}{\epsilon^2}+\frac{4}{\epsilon}\ln\left(\frac{\nu e^{-y_J}}{\mu}\right)+4\ln^2\left(\frac{\mu}{p_T^{\text{cut}}}\right) \right. \\ \left. +8\ln\left(\frac{\mu}{p_T^{\text{cut}}}\right)\ln\left(\frac{e^{-y_J}\nu}{\mu}\right)+\frac{\pi^2}{6}\right\}, \tag{B.22}$$

$$S^{\eta=0}_{aj,R_J\to 0} = \frac{\alpha_s}{4\pi}\left\{\left[-\frac{4}{\epsilon}-8\ln\left(\frac{\mu}{p_T^{\text{cut}}}\right)+8\ln(2)\right]\ln(2\pi)-8\ln\left(\frac{\mu}{p_T^{\text{cut}}}\right)\ln(2\pi) \right. \\ \left. +4\ln^2(\pi)-\frac{\pi^2}{3}-4\ln^2(2)\right\}, \tag{B.23}$$

thus completing the evaluation of S_{aj} in the small R_J limit. The S_{bj} contribution follows in exactly the same way and is related to the S_{aj} contribution via

$$S_{bj} = S_{aj}|_{y_J\to -y_J}\,. \tag{B.24}$$

Inserting the expressions for the integrals, we therefore find that the soft function up to one-loop order is given by

$$S_\kappa^{(1)} = (\mathbf{T}_a^2+\mathbf{T}_b^2)\left[-4\ln^2\left(\frac{\mu}{p_T^{\text{cut}}}\right)-8\ln\left(\frac{\mu}{p_T^{\text{cut}}}\right)\ln\left(\frac{\nu}{\mu}\right)-\frac{\pi^2}{6}\right] \\ +8y_J(\mathbf{T}_a^2-\mathbf{T}_b^2)\ln\left(\frac{\mu}{p_T^{\text{cut}}}\right)+\mathbf{T}_j^2\left[-4\ln^2 R_J+8\ln\left(\frac{\mu}{p_T^{\text{cut}}}\right)\ln R_J\right]. \tag{B.25}$$

JHEP03(2025)155

Including higher order terms from the expansion in ρ of each of the integrals on the r.h.s. of eq. (B.17), we find that the soft function including power corrections in R_J is given by

$$\begin{aligned} S_\kappa^{(1)} &= (\mathbf{T}_a^2 + \mathbf{T}_b^2)\left[-4\ln^2\left(\frac{\mu}{p_T^{\text{cut}}}\right) - 8\ln\left(\frac{\mu}{p_T^{\text{cut}}}\right)\ln\left(\frac{\nu}{\mu}\right) - \frac{\pi^2}{6} + 2R_J^2\ln\left(\frac{\mu}{p_T^{\text{cut}}R_J}\right) + R_J^2\right] \\ &\quad + 8y_J(\mathbf{T}_a^2 - \mathbf{T}_b^2)\ln\left(\frac{\mu}{p_T^{\text{cut}}}\right) \\ &\quad + \mathbf{T}_j^2\left[-4\ln^2 R_J + 8\ln\left(\frac{\mu}{p_T^{\text{cut}}}\right)\ln R_J - R_J^2\ln\left(\frac{\mu}{p_T^{\text{cut}}R_J}\right) + \frac{R_J^2}{6}\right]. \end{aligned} \tag{B.26}$$

C Resummation ingredients

The following functions enter in the evolution kernels in section 3.3.2:

$$\begin{aligned} K_\Gamma^i(\mu_0,\mu) &= \int_{\alpha_s(\mu_0)}^{\alpha_s(\mu)}\frac{\mathrm{d}\alpha_s}{\beta(\alpha_s)}\Gamma_{\text{cusp}}^i(\alpha_s)\int_{\alpha_s(\mu_0)}^{\alpha_s}\frac{\mathrm{d}\alpha_s'}{\beta(\alpha_s')}\,, \\ \eta_\Gamma^i(\mu_0,\mu) &= \int_{\alpha_s(\mu_0)}^{\alpha_s(\mu)}\frac{\mathrm{d}\alpha_s}{\beta(\alpha_s)}\Gamma_{\text{cusp}}^i(\alpha_s)\,, \\ K_\gamma^i(\mu_0,\mu) &= \int_{\alpha_s(\mu_0)}^{\alpha_s(\mu)}\frac{\mathrm{d}\alpha_s}{\beta(\alpha_s)}\gamma^i(\alpha_s)\,. \end{aligned} \tag{C.1}$$

Up to NNLL accuracy, their expressions are given by

$$\begin{aligned} K_\Gamma^i(\mu_0,\mu) &= -\frac{\Gamma_0^i}{4\beta_0^2}\left\{\frac{4\pi}{\alpha_s(\mu_0)}\left(1-\frac{1}{r}-\ln r\right) + \left(\frac{\Gamma_1}{\Gamma_0}-\frac{\beta_1}{\beta_0}\right)(1-r+\ln r)\right. \\ &\quad + \frac{\beta_1}{2\beta_0}\ln^2 r + \frac{\alpha_s(\mu_0)}{4\pi}\left[\left(\frac{\beta_1^2}{\beta_0^2}-\frac{\beta_2}{\beta_0}\right)\left(\frac{1-r^2}{2}+\ln r\right)\right. \\ &\quad \left.\left. + \left(\frac{\beta_1\Gamma_1}{\beta_0\Gamma_0}-\frac{\beta_1^2}{\beta_0^2}\right)(1-r+r\ln r) - \left(\frac{\Gamma_2}{\Gamma_0}-\frac{\beta_1\Gamma_1}{\beta_0\Gamma_0}\right)\frac{(1-r)^2}{2}\right]\right\}, \\ \eta_\Gamma^i(\mu_0,\mu) &= -\frac{\Gamma_0^i}{2\beta_0}\left[\ln r + \frac{\alpha_s(\mu_0)}{4\pi}\left(\frac{\Gamma_1}{\Gamma_0}-\frac{\beta_1}{\beta_0}\right)(r-1)\right. \\ &\quad \left. + \frac{\alpha_s^2(\mu_0)}{(4\pi)^2}\left(\frac{\Gamma_2}{\Gamma_0}-\frac{\beta_1\Gamma_1}{\beta_0\Gamma_0}+\frac{\beta_1^2}{\beta_0^2}-\frac{\beta_2}{\beta_0}\right)\frac{r^2-1}{2}\right], \\ K_\gamma^i(\mu_0,\mu) &= -\frac{\gamma_0^i}{2\beta_0}\left[\ln r + \frac{\alpha_s(\mu_0)}{4\pi}\left(\frac{\gamma_1^i}{\gamma_0^i}-\frac{\beta_1}{\beta_0}\right)(r-1)\right], \end{aligned} \tag{C.2}$$

where we defined $r = \alpha_s(\mu)/\alpha_s(\mu_0)$. The coefficients in the expansion of the cusp anomalous dimension in eq. (3.1) and β-function in eq. (3.2) that are needed up to NNLL$'$ are given by

$$\begin{aligned} \beta_0 &= \frac{11}{3}C_A - \frac{4}{3}T_F n_f\,, \\ \beta_1 &= \frac{34}{3}C_A^2 - 2T_F n_f\Big(\frac{10}{3}C_A + 2C_F\Big)\,, \\ \beta_2 &= \frac{2857}{54}C_A^3 + 2T_F n_f\Big(-\frac{1415}{54}C_A^2 - \frac{205}{18}C_F C_A + C_F^2\Big) + 4T_F^2 n_f^2\Big(\frac{79}{54}C_A + \frac{11}{9}C_F\Big)\,, \\ \Gamma_0^i &= 4C_i\,, \end{aligned} \tag{C.3}$$

JHEP03(2025)155

$$\Gamma_1^i = 4C_i\Big[C_A\Big(\frac{67}{9} - 2\zeta_2\Big) - \frac{20}{9}\,T_F\,n_f\Big]\,,$$
$$\Gamma_2^i = 4C_i\Big\{C_A^2\Big(\frac{245}{6} - \frac{268}{9}\zeta_2 + \frac{22}{3}\zeta_3 + 22\zeta_4\Big) + 2T_F\,n_f\Big[C_A\Big(-\frac{209}{27} + \frac{40}{9}\zeta_2 - \frac{28}{3}\zeta_3\Big) + C_F\Big(-\frac{55}{6} + 8\zeta_3\Big)\Big] - \frac{16}{27}\,T_F^2\,n_f^2\Big\}\,. \quad \text{(C.4)}$$

We sometimes use the colour-stripped coefficients $\Gamma_n = \Gamma_n^i/C_i$ for $n \leq 2$.

Data Availability Statement. This article has no associated data or the data will not be deposited.

Code Availability Statement. This article has no associated code or the code will not be deposited.

References

[1] ATLAS collaboration, *Observation of a new particle in the search for the Standard Model Higgs boson with the ATLAS detector at the LHC*, *Phys. Lett. B* **716** (2012) 1 [arXiv:1207.7214] [INSPIRE].

[2] CMS collaboration, *Observation of a New Boson at a Mass of 125 GeV with the CMS Experiment at the LHC*, *Phys. Lett. B* **716** (2012) 30 [arXiv:1207.7235] [INSPIRE].

[3] N. Berger et al., *Simplified Template Cross Sections - Stage 1.1*, arXiv:1906.02754 [INSPIRE].

[4] J.R. Andersen et al., *Les Houches 2015: Physics at TeV Colliders Standard Model Working Group Report*, in the proceedings of the *9th Les Houches Workshop on Physics at TeV Colliders*, Les Houches, France, June 01–19 (2015) [arXiv:1605.04692] [INSPIRE].

[5] LHC Higgs Cross Section Working Group collaboration, *Handbook of LHC Higgs Cross Sections: 4. Deciphering the Nature of the Higgs Sector*, arXiv:1610.07922 [DOI:10.23731/CYRM-2017-002] [INSPIRE].

[6] ATLAS collaboration, *A detailed map of Higgs boson interactions by the ATLAS experiment ten years after the discovery*, *Nature* **607** (2022) 52 [*Erratum ibid.* **612** (2022) E24] [arXiv:2207.00092] [INSPIRE].

[7] CMS collaboration, *Measurements of production cross sections of the Higgs boson in the four-lepton final state in proton–proton collisions at* $\sqrt{s} = 13$ *TeV*, *Eur. Phys. J. C* **81** (2021) 488 [arXiv:2103.04956] [INSPIRE].

[8] CMS collaboration, *Measurements of Higgs boson production cross sections and couplings in the diphoton decay channel at* $\sqrt{s} = 13$ *TeV*, *JHEP* **07** (2021) 027 [arXiv:2103.06956] [INSPIRE].

[9] I.W. Stewart, F.J. Tackmann and W.J. Waalewijn, *Factorization at the LHC: from PDFs to Initial State Jets*, *Phys. Rev. D* **81** (2010) 094035 [arXiv:0910.0467] [INSPIRE].

[10] I.W. Stewart, F.J. Tackmann and W.J. Waalewijn, *The Beam Thrust Cross Section for Drell-Yan at NNLL Order*, *Phys. Rev. Lett.* **106** (2011) 032001 [arXiv:1005.4060] [INSPIRE].

JHEP03(2025)155

[11] C.F. Berger et al., *Higgs Production with a Central Jet Veto at NNLL+NNLO*, *JHEP* **04** (2011) 092 [arXiv:1012.4480] [INSPIRE].

[12] A. Banfi, G.P. Salam and G. Zanderighi, *NLL+NNLO predictions for jet-veto efficiencies in Higgs-boson and Drell-Yan production*, *JHEP* **06** (2012) 159 [arXiv:1203.5773] [INSPIRE].

[13] T. Becher and M. Neubert, *Factorization and NNLL Resummation for Higgs Production with a Jet Veto*, *JHEP* **07** (2012) 108 [arXiv:1205.3806] [INSPIRE].

[14] F.J. Tackmann, J.R. Walsh and S. Zuberi, *Resummation Properties of Jet Vetoes at the LHC*, *Phys. Rev. D* **86** (2012) 053011 [arXiv:1206.4312] [INSPIRE].

[15] A. Banfi, P.F. Monni, G.P. Salam and G. Zanderighi, *Higgs and Z-boson production with a jet veto*, *Phys. Rev. Lett.* **109** (2012) 202001 [arXiv:1206.4998] [INSPIRE].

[16] I.W. Stewart, F.J. Tackmann, J.R. Walsh and S. Zuberi, *Jet p_T resummation in Higgs production at $NNLL' + NNLO$*, *Phys. Rev. D* **89** (2014) 054001 [arXiv:1307.1808] [INSPIRE].

[17] T. Becher, M. Neubert and L. Rothen, *Factorization and N^3LL_p+NNLO predictions for the Higgs cross section with a jet veto*, *JHEP* **10** (2013) 125 [arXiv:1307.0025] [INSPIRE].

[18] A. Banfi et al., *Jet-vetoed Higgs cross section in gluon fusion at N^3LO+NNLL with small-R resummation*, *JHEP* **04** (2016) 049 [arXiv:1511.02886] [INSPIRE].

[19] D.Y. Shao, C.S. Li and H.T. Li, *Resummation Prediction on Higgs and Vector Boson Associated Production with a Jet Veto at the LHC*, *JHEP* **02** (2014) 117 [arXiv:1309.5015] [INSPIRE].

[20] Y. Li and X. Liu, *High precision predictions for exclusive VH production at the LHC*, *JHEP* **06** (2014) 028 [arXiv:1401.2149] [INSPIRE].

[21] I. Moult and I.W. Stewart, *Jet Vetoes interfering with $H \to WW$*, *JHEP* **09** (2014) 129 [arXiv:1405.5534] [INSPIRE].

[22] P.F. Monni and G. Zanderighi, *On the excess in the inclusive $W^+W^- \to l^+l^-\nu\bar{\nu}$ cross section*, *JHEP* **05** (2015) 013 [arXiv:1410.4745] [INSPIRE].

[23] Y. Wang, C.S. Li and Z.L. Liu, *Resummation prediction on gauge boson pair production with a jet veto*, *Phys. Rev. D* **93** (2016) 094020 [arXiv:1504.00509] [INSPIRE].

[24] F.J. Tackmann, W.J. Waalewijn and L. Zeune, *Impact of Jet Veto Resummation on Slepton Searches*, *JHEP* **07** (2016) 119 [arXiv:1603.03052] [INSPIRE].

[25] M.A. Ebert et al., *Exploiting jet binning to identify the initial state of high-mass resonances*, *Phys. Rev. D* **94** (2016) 051901 [arXiv:1605.06114] [INSPIRE].

[26] S. Dawson et al., *Resummation of jet veto logarithms at N^3LL_a + NNLO for W^+W^- production at the LHC*, *Phys. Rev. D* **94** (2016) 114014 [arXiv:1606.01034] [INSPIRE].

[27] L. Arpino, A. Banfi, S. Jäger and N. Kauer, *BSM WW production with a jet veto*, *JHEP* **08** (2019) 076 [arXiv:1905.06646] [INSPIRE].

[28] S. Kallweit, E. Re, L. Rottoli and M. Wiesemann, *Accurate single- and double-differential resummation of colour-singlet processes with MATRIX+RADISH: W^+W^- production at the LHC*, *JHEP* **12** (2020) 147 [arXiv:2004.07720] [INSPIRE].

[29] J.M. Campbell, R.K. Ellis, T. Neumann and S. Seth, *Jet-veto resummation at N^3LL_p + NNLO in boson production processes*, *JHEP* **04** (2023) 106 [arXiv:2301.11768] [INSPIRE].

[30] J.K.L. Michel, P. Pietrulewicz and F.J. Tackmann, *Jet Veto Resummation with Jet Rapidity Cuts*, *JHEP* **04** (2019) 142 [arXiv:1810.12911] [INSPIRE].

JHEP03(2025)155

[31] S. Gangal, M. Stahlhofen and F.J. Tackmann, *Rapidity-Dependent Jet Vetoes*, *Phys. Rev. D* **91** (2015) 054023 [arXiv:1412.4792] [INSPIRE].

[32] S. Gangal, J.R. Gaunt, F.J. Tackmann and E. Vryonidou, *Higgs Production at NNLL′+NNLO using Rapidity Dependent Jet Vetoes*, *JHEP* **05** (2020) 054 [arXiv:2003.04323] [INSPIRE].

[33] A. Gavardi, M.A. Lim, S. Alioli and F.J. Tackmann, *NNLO+PS W^+W^- production using jet veto resummation at NNLL'*, *JHEP* **12** (2023) 069 [arXiv:2308.11577] [INSPIRE].

[34] S. Alioli et al., *Combining Higher-Order Resummation with Multiple NLO Calculations and Parton Showers in GENEVA*, *JHEP* **09** (2013) 120 [arXiv:1211.7049] [INSPIRE].

[35] S. Alioli et al., *Drell-Yan production at NNLL'+NNLO matched to parton showers*, *Phys. Rev. D* **92** (2015) 094020 [arXiv:1508.01475] [INSPIRE].

[36] X. Liu and F. Petriello, *Resummation of jet-veto logarithms in hadronic processes containing jets*, *Phys. Rev. D* **87** (2013) 014018 [arXiv:1210.1906] [INSPIRE].

[37] X. Liu and F. Petriello, *Reducing theoretical uncertainties for exclusive Higgs-boson plus one-jet production at the LHC*, *Phys. Rev. D* **87** (2013) 094027 [arXiv:1303.4405] [INSPIRE].

[38] R. Boughezal et al., *Combining Resummed Higgs Predictions Across Jet Bins*, *Phys. Rev. D* **89** (2014) 074044 [arXiv:1312.4535] [INSPIRE].

[39] F.J. Tackmann, *Beyond Scale Variations: Perturbative Theory Uncertainties from Nuisance Parameters*, arXiv:2411.18606 [INSPIRE].

[40] X. Chen et al., *NNLO QCD corrections to Higgs boson production at large transverse momentum*, *JHEP* **10** (2016) 066 [arXiv:1607.08817] [INSPIRE].

[41] K. Becker et al., *Precise predictions for boosted Higgs production*, *SciPost Phys. Core* **7** (2024) 001 [arXiv:2005.07762] [INSPIRE].

[42] M. Dasgupta, F. Dreyer, G.P. Salam and G. Soyez, *Small-radius jets to all orders in QCD*, *JHEP* **04** (2015) 039 [arXiv:1411.5182] [INSPIRE].

[43] C.W. Bauer, S. Fleming, D. Pirjol and I.W. Stewart, *An effective field theory for collinear and soft gluons: heavy to light decays*, *Phys. Rev. D* **63** (2001) 114020 [hep-ph/0011336] [INSPIRE].

[44] C.W. Bauer and I.W. Stewart, *Invariant operators in collinear effective theory*, *Phys. Lett. B* **516** (2001) 134 [hep-ph/0107001] [INSPIRE].

[45] C.W. Bauer, D. Pirjol and I.W. Stewart, *Soft collinear factorization in effective field theory*, *Phys. Rev. D* **65** (2002) 054022 [hep-ph/0109045] [INSPIRE].

[46] C.W. Bauer et al., *Hard scattering factorization from effective field theory*, *Phys. Rev. D* **66** (2002) 014017 [hep-ph/0202088] [INSPIRE].

[47] M. Beneke, A.P. Chapovsky, M. Diehl and T. Feldmann, *Soft collinear effective theory and heavy to light currents beyond leading power*, *Nucl. Phys. B* **643** (2002) 431 [hep-ph/0206152] [INSPIRE].

[48] Y.-T. Chien, A. Hornig and C. Lee, *Soft-collinear mode for jet cross sections in soft collinear effective theory*, *Phys. Rev. D* **93** (2016) 014033 [arXiv:1509.04287] [INSPIRE].

[49] S. Alioli and J.R. Walsh, *Jet Veto Clustering Logarithms Beyond Leading Order*, *JHEP* **03** (2014) 119 [arXiv:1311.5234] [INSPIRE].

[50] A.J. Larkoski, I. Moult and D. Neill, *Non-Global Logarithms, Factorization, and the Soft Substructure of Jets*, *JHEP* **09** (2015) 143 [arXiv:1501.04596] [INSPIRE].

JHEP03(2025)155

[51] T. Becher, M. Neubert, L. Rothen and D.Y. Shao, *Effective Field Theory for Jet Processes*, *Phys. Rev. Lett.* **116** (2016) 192001 [arXiv:1508.06645] [INSPIRE].

[52] S. Gangal, J.R. Gaunt, M. Stahlhofen and F.J. Tackmann, *Two-Loop Beam and Soft Functions for Rapidity-Dependent Jet Vetoes*, *JHEP* **02** (2017) 026 [arXiv:1608.01999] [INSPIRE].

[53] S.D. Ellis et al., *Jet Shapes and Jet Algorithms in SCET*, *JHEP* **11** (2010) 101 [arXiv:1001.0014] [INSPIRE].

[54] A. Banfi, F.A. Dreyer and P.F. Monni, *Next-to-leading non-global logarithms in QCD*, *JHEP* **10** (2021) 006 [arXiv:2104.06416] [INSPIRE].

[55] T. Becher, N. Schalch and X. Xu, *Resummation of Next-to-Leading Nonglobal Logarithms at the LHC*, *Phys. Rev. Lett.* **132** (2024) 081602 [arXiv:2307.02283] [INSPIRE].

[56] T. Becher, G. Bell, C. Lorentzen and S. Marti, *Transverse-momentum spectra of electroweak bosons near threshold at NNLO*, *JHEP* **02** (2014) 004 [arXiv:1309.3245] [INSPIRE].

[57] I. Moult, I.W. Stewart, F.J. Tackmann and W.J. Waalewijn, *Employing Helicity Amplitudes for Resummation*, *Phys. Rev. D* **93** (2016) 094003 [arXiv:1508.02397] [INSPIRE].

[58] C.R. Schmidt, $H \to ggg(gq\bar{q})$ *at two loops in the large* M_t *limit*, *Phys. Lett. B* **413** (1997) 391 [hep-ph/9707448] [INSPIRE].

[59] T. Gehrmann, M. Jaquier, E.W.N. Glover and A. Koukoutsakis, *Two-Loop QCD Corrections to the Helicity Amplitudes for* $H \to 3$ *partons*, *JHEP* **02** (2012) 056 [arXiv:1112.3554] [INSPIRE].

[60] E. Gardi and L. Magnea, *Factorization constraints for soft anomalous dimensions in QCD scattering amplitudes*, *JHEP* **03** (2009) 079 [arXiv:0901.1091] [INSPIRE].

[61] H.-Y. Liu, X. Liu and S.-O. Moch, *Anti-kT jet function at next-to-next-to-leading order*, *Phys. Rev. D* **104** (2021) 014016 [arXiv:2103.08680] [INSPIRE].

[62] S. Abreu et al., *Quark and gluon two-loop beam functions for leading-jet* p_T *and slicing at NNLO*, *JHEP* **04** (2023) 127 [arXiv:2207.07037] [INSPIRE].

[63] S. Abreu, J.R. Gaunt, P.F. Monni and R. Szafron, *The analytic two-loop soft function for leading-jet* p_T, *JHEP* **08** (2022) 268 [arXiv:2204.02987] [INSPIRE].

[64] G. Bell, K. Brune, G. Das and M. Wald, *The NNLO quark beam function for jet-veto resummation*, *JHEP* **01** (2023) 083 [arXiv:2207.05578] [INSPIRE].

[65] G. Bell et al., *The NNLO gluon beam function for jet-veto resummation*, *JHEP* **07** (2024) 014 [arXiv:2403.15247] [INSPIRE].

[66] Y. Hatta and T. Ueda, *Resummation of non-global logarithms at finite* N_c, *Nucl. Phys. B* **874** (2013) 808 [arXiv:1304.6930] [INSPIRE].

[67] M. Dasgupta and G.P. Salam, *Resummation of nonglobal QCD observables*, *Phys. Lett. B* **512** (2001) 323 [hep-ph/0104277] [INSPIRE].

[68] A. Banfi, G. Marchesini and G. Smye, *Away from jet energy flow*, *JHEP* **08** (2002) 006 [hep-ph/0206076] [INSPIRE].

[69] M.D. Schwartz and H.X. Zhu, *Nonglobal logarithms at three loops, four loops, five loops, and beyond*, *Phys. Rev. D* **90** (2014) 065004 [arXiv:1403.4949] [INSPIRE].

[70] S. Alioli et al., *Refining the GENEVA method for Higgs boson production via gluon fusion*, *JHEP* **05** (2023) 128 [arXiv:2301.11875] [INSPIRE].

[71] Z. Ligeti, I.W. Stewart and F.J. Tackmann, *Treating the b quark distribution function with reliable uncertainties*, *Phys. Rev. D* **78** (2008) 114014 [arXiv:0807.1926] [INSPIRE].

JHEP03(2025)155

[72] R. Abbate et al., *Thrust at N^3LL with Power Corrections and a Precision Global Fit for $\alpha_s(mZ)$*, *Phys. Rev. D* **83** (2011) 074021 [arXiv:1006.3080] [INSPIRE].

[73] P.F. Monni, T. Gehrmann and G. Luisoni, *Two-Loop Soft Corrections and Resummation of the Thrust Distribution in the Dijet Region*, *JHEP* **08** (2011) 010 [arXiv:1105.4560] [INSPIRE].

[74] S. Bailey et al., *Parton distributions from LHC, HERA, Tevatron and fixed target data: MSHT20 PDFs*, *Eur. Phys. J. C* **81** (2021) 341 [arXiv:2012.04684] [INSPIRE].

[75] I.W. Stewart and F.J. Tackmann, *Theory Uncertainties for Higgs and Other Searches Using Jet Bins*, *Phys. Rev. D* **85** (2012) 034011 [arXiv:1107.2117] [INSPIRE].

[76] S.P. Jones, M. Kerner and G. Luisoni, *Next-to-Leading-Order QCD Corrections to Higgs Boson Plus Jet Production with Full Top-Quark Mass Dependence*, *Phys. Rev. Lett.* **120** (2018) 162001 [*Erratum ibid.* **128** (2022) 059901] [arXiv:1802.00349] [INSPIRE].

[77] M. Czakon et al., *Quark mass effects in Higgs production*, *JHEP* **10** (2024) 210 [arXiv:2407.12413] [INSPIRE].

[78] V. Ahrens et al., *Renormalization-Group Improved Predictions for Top-Quark Pair Production at Hadron Colliders*, *JHEP* **09** (2010) 097 [arXiv:1003.5827] [INSPIRE].

[79] S. Alioli, A. Broggio and M.A. Lim, *Zero-jettiness resummation for top-quark pair production at the LHC*, *JHEP* **01** (2022) 066 [arXiv:2111.03632] [INSPIRE].

[80] A. Gao, H.T. Li, I. Moult and H.X. Zhu, *The transverse energy-energy correlator at next-to-next-to-next-to-leading logarithm*, *JHEP* **09** (2024) 072 [arXiv:2312.16408] [INSPIRE].

JHEP03(2025)155